Anthropogenic CO_2 inventory of the Indian Ocean

C. L. Sabine,[1] R. M. Key,[1] K. M. Johnson,[2] F. J. Millero,[3] A. Poisson,[4] J. L. Sarmiento,[1] D. W. R. Wallace,[2,5] and C. D. Winn[6,7]

Abstract. This study presents basin-wide anthropogenic CO_2 inventory estimates for the Indian Ocean based on measurements from the World Ocean Circulation Experiment/Joint Global Ocean Flux Study global survey. These estimates employed slightly modified ΔC^* and time series techniques originally proposed by *Gruber et al.* [1996] and *Wallace* [1995], respectively. Together, the two methods yield the total oceanic anthropogenic CO_2 and the carbon increase over the past 2 decades. The highest concentrations and the deepest penetrations of anthropogenic carbon are associated with the Subtropical Convergence at around 30° to 40°S. With both techniques, the lowest anthropogenic CO_2 column inventories are observed south of 50°S. The total anthropogenic CO_2 inventory north of 35°S was 13.6±2 Pg C in 1995. The inventory increase since GEOSECS (Geochemical Ocean Sections Program) was 4.1±1 Pg C for the same area. Approximately 6.7±1 Pg C are stored in the Indian sector of the Southern Ocean, giving a total Indian Ocean inventory of 20.3 ±3 Pg C for 1995. These estimates are compared to anthropogenic CO_2 inventories estimated by the Princeton ocean biogeochemistry model. The model predicts an Indian Ocean sink north of 35°S that is only 0.61-0.68 times the results presented here; while the Southern Ocean sink is nearly 2.6 times higher than the measurement-based estimate. These results clearly identify areas in the models that need further examination and provide a good baseline for future studies of the anthropogenic inventory.

1. Introduction

The current Intergovernmental Panel on Climate Change (IPCC) estimate for the oceanic sink of anthropogenic CO_2 (2.0 ±0.8 Pg C yr^{-1}) is based primarily on ocean models [e.g., *Sarmiento et al.*, 1992; *Sarmiento and Sundquist*, 1992; *Siegenthaler and Sarmiento*, 1993; *Siegenthaler and Joos*, 1992; *Stocker et al.*, 1994], atmospheric models [e.g., *Keeling et al.*, 1989; *Keeling and Shertz*, 1992] or on the oceanic distribution of related species such as $\delta^{13}C$ [*Quay et al.*, 1992]. Although the basic assumptions used in these methods are reasonably well grounded, there will always be room for doubt with indirect approaches. Direct estimates of the oceanic CO_2 sink, however, have been primarily limited by a lack of high-quality data on a global scale.

Two general approaches can be used to estimate the uptake of anthropogenic CO_2 by the oceans. One approach, initially proposed by *Tans et al.* [1990], is to use direct measurements of the air-sea difference in CO_2 partial pressure together with global winds and a gas exchange coefficient to estimate the net transfer of CO_2 into the oceans. These estimates, together with an atmospheric transport model, predicted that the oceanic sink was only 0.3 to 0.8 Pg C yr^{-1}, much smaller than the model predictions. The difficulty with the ΔpCO_2 approach lies both in the large uncertainty in the wind speed dependence of the air-sea gas exchange velocity and in the ability to properly represent the large temporal and spatial variability of the surface ocean pCO_2 because of a lack of seasonal, global data coverage. This estimate has recently been revised to 0.6 to 1.34 Pg C yr^{-1} with the addition of more data and a lateral advection-diffusion transport equation to help with the necessary temporal and spatial interpolations [*Takahashi et al.*, 1997].

A second approach, which avoids many of the problems of temporal variability, is to estimate the inventory of anthropogenic CO_2 stored in the oceans interior based on inorganic carbon measurements. Again, the problem with this approach in the past has been a lack of high-quality global data coverage. As pointed out by *Broecker et al.* [1979] after completion of the last global oceanographic survey, GEOSECS (Geochemical Ocean Sections Program), the precision of ocean carbon measurements at that time was two orders of magnitude smaller than the predicted 0.035% annual increase in surface ocean dissolved inorganic carbon. Nearly 20 years have passed since GEOSECS, and the quality of today's carbon measurements has improved significantly.

This is the first of several papers aimed at estimating the anthropogenic CO_2 inventory of the oceans based on the recent global survey of CO_2 in the oceans. The survey was conducted as part of the JGOFS (Joint Global Ocean Flux Study) in close cooperation with the WOCE-HP (World Ocean Circulation Experiment - Hydrographic Programme). This program was a multiyear effort to collect high-precision inorganic carbon data with the highest possible spatial resolution on a global scale. This paper will focus on anthropogenic CO_2 estimates for the Indian Ocean. Papers will

[1]Department of Geosciences, Princeton University, Princeton, New Jersey.

[2]Oceanographic and Atmospheric Sciences Division, Brookhaven National Laboratory, Upton, New York.

[3]Rosenstiel School of Marine and Atmospheric Science, University of Miami, Miami, Florida.

[4]Laboratoire de Physique et Chimie Marines, Université Pierre et Marie Curie, Paris.

[5]Now at Institut für Meereskunde, Universität Kiel.

[6]Department of Oceanography, University of Hawaii at Manoa, Honolulu, Hawaii.

[7]Now at Hawaii Pacific University, Kaneohe, Hawaii.

soon follow with estimates for the other major ocean basins, with the ultimate goal of generating an estimate of the global oceanic anthropogenic CO_2 sink based on direct carbon system measurements. The strength of these calculations lies not only in our ability to directly estimate the magnitude of the oceanic anthropogenic CO_2 sink but also in the fact that these estimates can be directly compared to anthropogenic CO_2 inventories estimated by carbon-cycle ocean general circulation models (GCMs). The two methods described here provide information over different timescales. The combined results place strong constraints on the uptake rate for anthropogenic CO_2 and are useful for identifying weaknesses in the models.

2. Methods

Estimates of the anthropogenic CO_2 inventory are determined from measured values using two different techniques. The first technique, referred to as the "time series" approach, is based on quantifying the increase in total carbon dioxide (TCO_2) since GEOSECS. The second approach quantifies the total anthropogenic CO_2 inventory using a quasi-conservative tracer, ΔC^*. Although the general idea for both techniques has been around for a long time, recent improvements in the estimation of the preserved end-member concentrations together with significant improvements in the accuracy and spatial coverage of global carbon data give us much more confidence in these results. Given the difficulty of isolating the anthropogenic signal from the large TCO_2 background, however, it is relevant to summarize the quality of the carbon data set and the techniques used to estimate the anthropogenic signal.

2.1. Data Quality

Over 20,000 water samples collected between December 1994 and July 1996 as part of the U.S. WOCE Indian Ocean survey were analyzed for both TCO_2 and total alkalinity (TA) using standard coulometric and potentiometric techniques, respectively. Figure 1 shows the locations of the 1352 stations occupied by U.S. WOCE as part of the Indian Ocean survey together with the station locations from the GEOSECS Indian Ocean Survey and the French INDIGO I, II, and III and CIVA1 (WOCE designation I6S) cruises. Details of the WOCE/JGOFS Indian Ocean CO_2 measurement program, including personnel, sampling procedures, measurement protocols and data quality assurance/quality control checks are described elsewhere [Johnson et al., 1998; Millero et al., 1998a]. Calibrations of both the TCO_2 and TA systems were checked approximately every 12 hours by analyzing Certified Reference Material (CRM) samples with known concentrations of TCO_2 and TA [Dickson, 1990] (A.G. Dickson, Oceanic carbon dioxide quality control at http://www-mpl.ucsd.edu/people/adickson/CO2_QC/, 1998). On the basis of these CRM analyses the accuracy of the TCO_2 and TA measurements was estimated to be ±2 and ±4 μmol kg⁻¹, respectively. Primary hydrographic data from the conductivity-temperature-depth/Rosette were collected and analyzed following standard procedures [Millard, 1982]. Samples were collected for salinity on every bottle and analyzed with an Autosal salinometer using standard techniques [UNESCO, 1981]. Oxygen samples were analyzed with an automated system using a modified Winkler technique [Culberson et al., 1991]. Nutrients were analyzed on a four-channel Technicon AutoAnalyzer II following the methods of Gordon et al. [1992]. Chlorofluorocarbon samples were analyzed
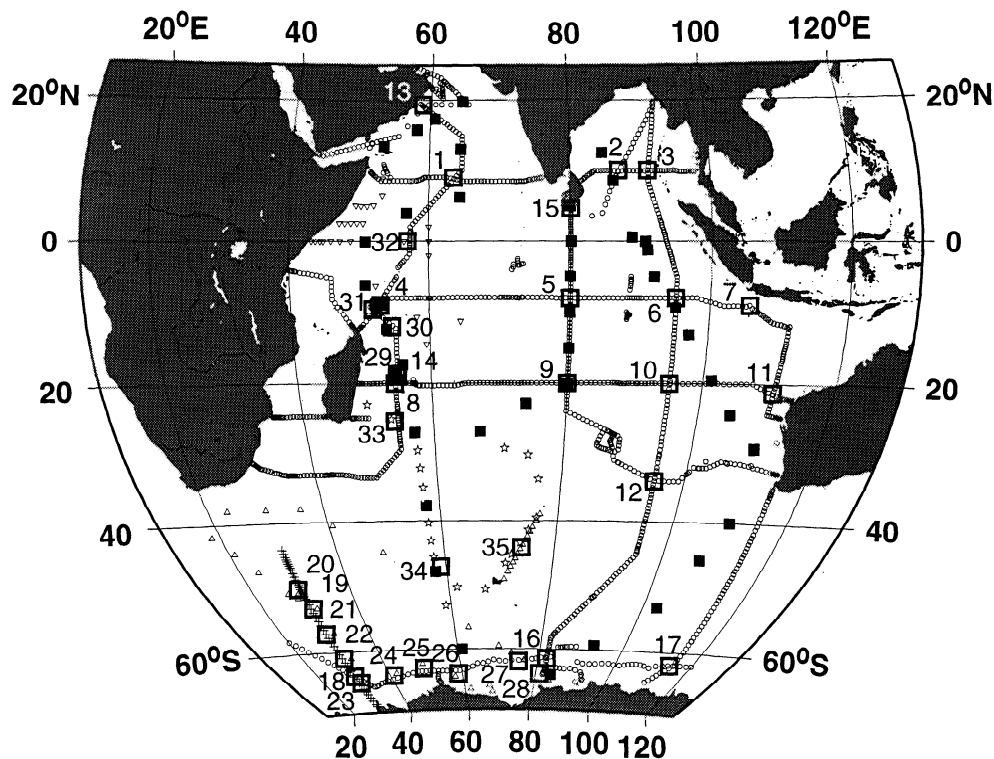

Figure 1. Station locations for WOCE Indian Ocean (circles), CIVA 1/I6S (crosses), INDIGO I (stars), INDIGO II (inverted triangles), INDIGO III (triangles), and GEOSECS (solid squares) Indian Ocean Surveys. Numbered boxes indicate location of crossovers discussed in the text. Map generated using Generic Mapping Tools version 3 [Wessel and Smith, 1995].

on a gas chromatograph using the techniques of *Bullister and Weiss* [1988]. Complete details of the analytical protocols and personnel can be obtained from the individual cruise reports available through the WOCE Office.

All of the data available at the time this manuscript was written have been included in the Indian Ocean analysis. For the primary hydrographic and nutrient data this means that the preliminary values available at the conclusion of the cruise were used. While we would prefer to use the final hydrographic data, typical postcruise corrections for the WOCE data sets are well below noise level for these calculations. Preliminary to semifinal chlorofluorocarbon (CFC) data were used to estimate the water age necessary for one of the correction terms in the ΔC^* method. Although postcruise blank corrections can influence the final CFC concentrations, an examination of the existing data (except I8N15E because data were not available at time of writing) indicated that the CFC-11 and CFC-12 age comparisons as well as comparisons of the data from one leg to the next were reasonably consistent with each other. The calculations were limited to waters with CFC-12 ages of less than 40 years where potential blank corrections are a relatively small fraction of the signal and mixing effects are minimized. The carbon data, which primarily influence the quality of the calculations, have all been calibrated and finalized as discussed briefly below.

Examination of Figure 1 reveals that although the WOCE survey was extensive, a large data gap exists in the southwestern Indian Ocean. To fill in this gap, data from the three French survey legs INDIGO I (February-March 1985), II (April 1986) and III (January-February 1987) as well as the more recent French cruise CIVA1 (February-March 1993 (WOCE designation I6S)) were included in the analysis [*Poisson et al.*, 1988; 1989; 1990]. TCO_2 and TA were analyzed on the INDIGO cruises using standard potentiometric titration techniques developed by *Edmond* [1970]. Potentiometric titrations were also used to analyze the TA samples on CIVA1, but the TCO_2 samples were analyzed using the coulometric techniques of *Johnson et al.* [1985]. The internal consistency of these cruises was examined by comparing carbon values in the deep waters (pressure > 2500 dbars) at the intersections of different legs. The stations selected for each crossover were those with carbon values which were closest to the intersection point. Smooth curves were fit through the data from each cruise as a function of sigma- 3 (density anomaly referenced to 3000 dbars) using Cleveland's loess function [*Cleveland and Devlin*, 1988; *Cleveland et al.*, 1992]. The difference between the curves was evaluated at 50 evenly spaced intervals that covered the density range over which the two data sets overlapped. The mean and standard deviation of the difference in TA and TCO_2 at the 35 intersections identified in Figure 1 are shown in Figure 2. The long-term stability of the WOCE/JGOFS measurements can be estimated from the first 17 crossover results. The mean of the absolute values for the leg-to-leg differences was less than the estimated accuracy for both TCO_2 (1.8 ±0.8 μmol kg^{-1}) and TA (2.4 ±1.6 μmol kg^{-1}). Although there is only one reliable crossover point between the WOCE/JGOFS cruises and the CIVA1 (I6S) cruise, the differences for both parameters are within the estimated accuracy of the measurements. Results from the analysis of CRM samples on the CIVA1 cruise also support the quality of the measurements. Some of the older INDIGO cruises, however, did appear to have offsets relative to the WOCE/JGOFS and CIVA1 data. INDIGO I and II alkalinity values averaged 6.5 μmol kg^{-1} high and 6.8 μmol kg^{-1} low, respectively, while the INDIGO III alkalinity values showed no clear offset. The INDIGO TCO_2 values were all consistently high relative

to WOCE/JGOFS and CIVA1, with differences of 10.7, 9.4, and 6.4 μmol kg^{-1}, respectively. These offsets are consistent with differences observed between at-sea values and replicate samples run at C.D. Keeling's shore-based TCO_2 facility (P. Guenther, personal communication, 1998). Since the INDIGO cruises were run prior to the introduction of CRMs, these offsets were presumed to be calibration differences, and each leg was adjusted to bring the values in line with the remaining cruises. The dotted boxes in Figure 2 show the original offsets at the crossovers. The solid boxes show the final offsets used in the following calculations. The means of the absolute values for the leg-to-leg differences for all 35 crossover analyses suggest that the final data set is internally consistent to ± 2.2 and 3.0 μmol kg^{-1} for TCO_2 and TA, respectively.

2.2. "Time Series" Calculations

The "time series" method for estimating the increase in the anthropogenic inventory uses measurements of TCO_2 made at a certain point in time to develop a predictive equation based on a multiple linear regression of the observed TCO_2 and simultaneously measured parameters such as temperature, salinity, oxygen, and TA (or silicate). These empirical multiparameter relationships have been shown to hold over large spatial scales, and their use drastically reduces the complicating effects of natural variability in determining temporal trends [*Brewer et al.*, 1995; *Wallace*, 1995; *Brewer et al.*, 1997]. The TCO_2 residuals from such predictive equations can be compared directly with patterns of residuals evaluated using the same predictive equation with TA, oxygen, and hydrographic data collected at different times (e.g., over decadal intervals). Since the uptake of anthropogenic CO_2 will increase the TCO_2 of the waters but will not directly affect the concentrations of the fit parameters, systematic changes in the magnitude and distribution of the TCO_2 residuals over time provide a direct estimate of the oceanic CO_2 inventory change due to the uptake of anthropogenic CO_2. The most comprehensive historical carbon data set for the Indian Ocean is from the GEOSECS expedition. By examining the WOCE data relative to that collected during the 1977-1978 GEOSECS Indian Ocean Survey, the increase in anthropogenic inventory over the last 18 years can be estimated.

2.2.1. GEOSECS fit. All of the GEOSECS data from the Indian Ocean (excluding Gulf of Aden and Red Sea regions) were fit with a single predictive equation as a function of potential temperature (θ), salinity (S), apparent oxygen utilization (AOU), and TA. To minimize the influence of short-term temporal variability, only data from pressures greater than 200 dbars were included in the fit. Despite the large area covered, the GEOSECS TCO_2 values can be predicted from this equation to ± 5.2 μmol kg^{-1} ($R^2 = 0.992$ and $N = 1120$). There is, however, a pattern in the residuals that correlates with observed hydrographic regions in the Indian Ocean (Figure 3).

In an attempt to improve the fit, a categorical variable based on region was added to the regression. The categorical variable differs from the other continuous variables by the fact that it is either applied or not applied depending on whether the sample is located within the region. The regions were defined as follows: 1, Arabian Sea (north of 10°N and west of 78°E); 2, North of 10°S (excluding Arabian Sea); 3, Chemical Front (21°S to 10°S); 4, Central Gyre (35°S to 21°S); and 5, Southern Ocean (south of 35°S)

The addition of the regional variable resulted in a marginal improvement in the fit ($R^2 = 0.993$ and σ = 4.9 μmol kg^{-1}) but

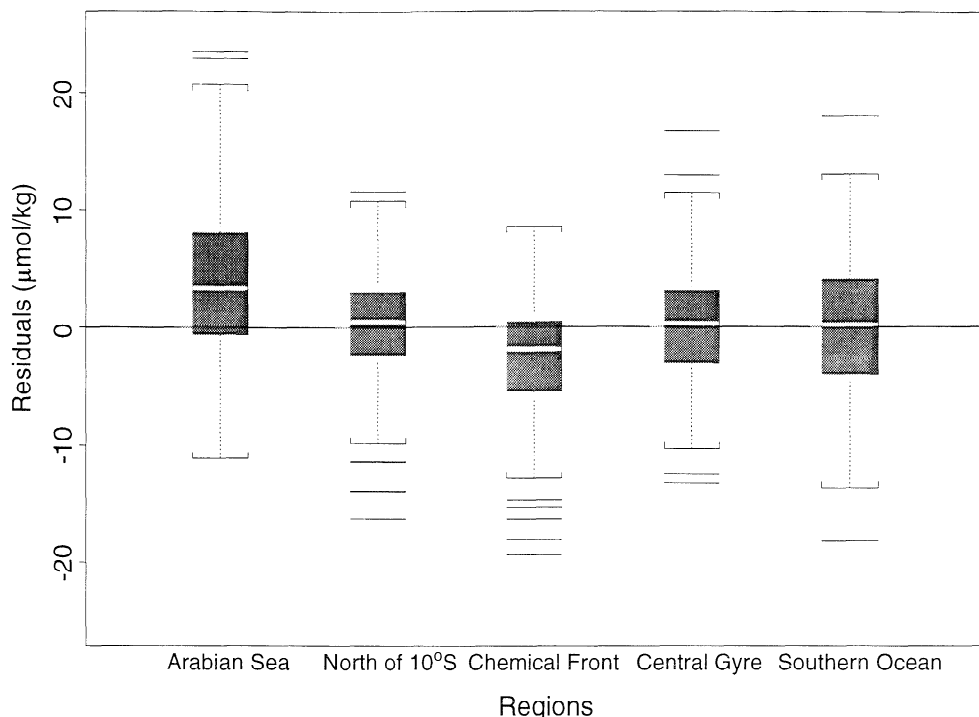**Figure 2.** Mean difference between deep water values of (a) TA and (b) TCO$_2$ for cruise intersections identified in Figure 1. Bars indicate one standard deviation. Dotted boxes indicate difference before adjustment (see explanation in text).

more importantly, removed the regional bias in the predictive equation. The coefficients of the final fit are shown in Figure 4 along with a plot of the measured versus calculated TCO$_2$ values for all of the points used in the fit. The resulting equation was then used to generate TCO$_2$ values for each of the WOCE sample locations based on the measured temperature, salinity, oxygen, and TA

values. The difference between the measured TCO$_2$ and the predicted TCO$_2$ reflects the CO$_2$ increase in the time between the two cruises. For this work the difference is referred to as "excess CO$_2$."

The residual method of estimating excess CO$_2$ was applied to the water column below 200 dbars. The surface waters, however, are dominated by seasonal variability which can bias the residual

Figure 3. Box and whiskers plot of residuals from a multiple linear regression of GEOSECS Indian Ocean data (pressure > 200 dbars) fit without the regional designator versus oceanographic region: $TCO_2 = 706.5 +$ $7.7S - 6.68\theta + 0.513TA + 0.7257AOU$. Solid boxes cover the range of $\pm$ 1 standard deviation about the mean. White lines within the boxes indicate median values. The whiskers indicate the range of data within the 99% confidence interval. The bars outside the whiskers give the values of outliers in the data set.
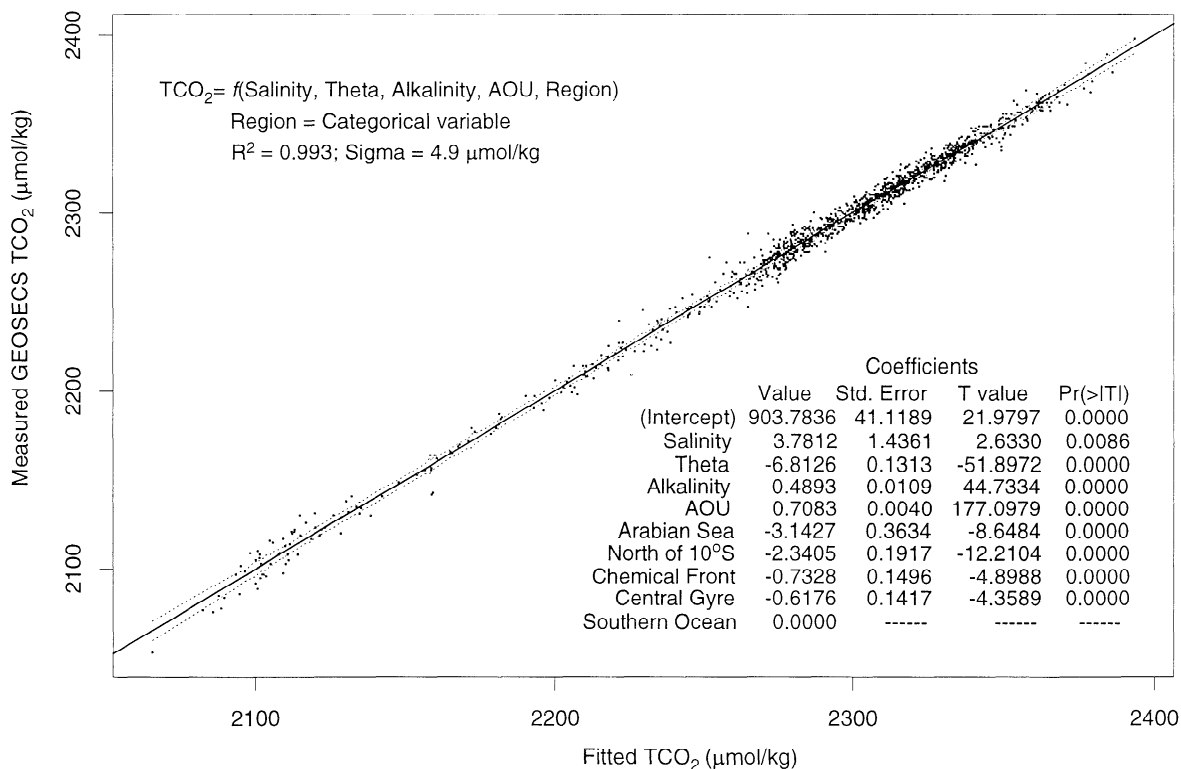
Figure 4. Plot of measured GEOSECS TCO_2 versus the calculated values. Solid line shows 1:1 relationship. The dashed lines indicate the 99% confidence interval for the fit. Text gives coefficients and related statistics. The column labeled "Pr(>|T|)" gives the probability that the T value in the previous column is larger than the T table value in a student T test.

calculations. The excess CO_2 of the surface waters therefore was determined from the difference in the estimated annual mean TCO_2 concentrations between GEOSECS and WOCE. The annual mean TCO_2 concentration was calculated from TA and surface water fCO_2. The surface alkalinity was estimated from the gridded annual mean salinity and temperature values of *Levitus et al.* [1994] and *Levitus and Boyer* [1994] using a multiple linear fit of the WOCE/JGOFS surface (pressure < 60 dbars) TA data to the measured surface temperature and salinity. The 1978 and 1995 surface water fCO_2 concentrations were estimated from the annual mean atmospheric concentration for the 2 years, and the annual mean ΔpCO_2 values estimated from the full correction scheme of *Takahashi et al.* [1997]. The excess TCO_2 values between the surface and 200 dbars were estimated with a linear approximation between the surface and 200 dbars values for each 1° grid box.

2.2.2. Data consistency.
One of the major concerns with the time series technique is the necessity of having two data sets that are consistent with each other. This consistency can be well documented for both TCO_2 and TA today through the use of certified reference materials (CRMs) supplied by A. Dickson of Scripps Institute of Oceanography (SIO). Since CRMs were not available at the time of GEOSECS, the only way to infer consistency with the WOCE data set is to assume the deep water carbon distributions have not changed since GEOSECS. The most reliable way to compare the two data sets is to examine the difference between the predicted TCO_2 and the measured TCO_2 (excess CO_2) in deep waters. The basic assumption with this technique is that the correlation between the different hydrographic parameters in the deep waters does not change with time. Given the long residence time of the deep and bottom waters in the ocean, this should be a reasonable assumption. This technique has the advantage that it implicitly accounts for the possibility of real variability in hydrographic properties between the two expeditions which would not be taken into account by simply comparing carbon profiles.

Examination of the excess CO_2 values in waters that should be free of anthropogenic CO_2 (pressures > 2000 dbars and containing no detectable chlorofluorocarbons) revealed that the GEOSECS values were 22.5 ±3 μmol kg^{-1} higher than the comparable WOCE measurements. This difference is comparable to the correction of -18 ± 7 μmol kg^{-1} noted by *Weiss et al.* [1983] to make the TCO_2 measurements consistent with the TA and discrete CO_2 partial pressure measurements based on the *Merbach et al.* [1973] dissociation constants. Additional support for an adjustment of the original GEOSECS data comes from C. D. Keeling's shore-based analysis of TCO_2 samples collected on both the GEOSECS and the WOCE/JGOFS expeditions. *Weiss et al.* [1983] point out that the shore-based analyses of Keeling were systematically smaller than the at-sea measurements by 16.5 ± 5 μmol kg^{-1} during GEOSECS. Similar comparisons between the WOCE/JGOFS at-sea measurements with Keeling's shore-based analyses indicate that the shore-based samples are approximately 5 μmol kg^{-1} higher than the at-sea values (P. Guenther, personal communication, 1998). Together, the GEOSECS-Keeling-WOCE/JGOFS combination suggests an offset of 21.5 μmol kg^{-1} between GEOSECS and WOCE/JGOFS at-sea measurements. It is also important to note that there is no indication of a depth or concentration dependent correction for the GEOSECS data. The shore-based comparison, based only on samples collected at the surface, is within 1 μmol kg^{-1} of the deep comparison described above. On the basis of these results a constant correction of the -22.5 μmol kg^{-1} was applied to the GEO-

SECS TCO_2 values to improve the consistency of the two data sets.

Ideally, the data used in the time series calculations would cover the same geographic region with as much of a time difference as possible. The trade-off, however, is that the quality and spatial coverage of the older data sets is generally very limited. Given the relatively small area of overlap between the WOCE/JGOFS and INDIGO data sets and the shorter time difference between cruises (9 years versus 18 years for WOCE - GEOSECS), the time series analysis was limited to a comparison between WOCE/JGOFS and GEOSECS in the main Indian Ocean basin.

2.2.3. Evaluation of Errors.
An estimate of the random errors associated with the excess CO_2 calculation can be made with a simple propagation of errors based on the fit to the GEOSECS data and the estimated precision of the WOCE/JGOFS data. With a standard deviation of 4.9 μmol kg^{-1} for the GEOSECS fit and an estimated long-term precision of ±2 μmol kg^{-1} in the WOCE/JGOFS TCO_2 values the excess CO_2 error is estimated to be approximately ±5 μmol kg^{-1}. This value compares well with the standard deviation of 3.5 μmol kg^{-1} for the excess CO_2 below the maximum anthropogenic CO_2 penetration depth (pressure > 1500 dbars).

Systematic errors with this technique are very difficult to evaluate. The largest potential systematic error is probably associated with the surface water estimates. Because the same ΔpCO_2 value is used to estimate the TCO_2 for both years, the excess CO_2 (1995 TCO_2 - 1978 TCO_2) is not very sensitive to potential errors associated with the actual ΔpCO_2 values used. The surface estimate is sensitive, however, to the assumption that the ΔpCO_2 has not changed over time (i.e., that the surface ocean increase has kept pace with the atmospheric increase). It is not likely that the surface ocean has increased at a faster rate than the atmosphere, but it is conceivable that the rate is slower. The current assumption results in a total inventory of 0.8 Pg C in the surface layer. If the surface ocean were increasing at half the rate of the atmosphere, the systematic bias in the final inventory would be around 0.4 Pg C. Below the surface layer the most likely systematic error would result from the uncertainty in fitting the GEOSECS data. Systematic errors associated with calibration differences between cruises are potentially quite large, but the analysis and subsequent correction given in section 2.2.2 should remove these biases. The estimated uncertainty for the GEOSECS adjustment was ±3 μmol kg^{-1}. If this value is integrated for the area north of 35°S between 200 m and the average penetration depth of the excess CO_2 (~ 800 m), the potential error would be ±0.9 Pg C. Propagating the errors for the surface and deeper layers gives an estimated error of approximately ±1 Pg C in the total excess CO_2 inventory. Clearly, there are other ways of estimating the potential errors in these calculations, but we feel that this is a reasonable estimate based on the available data.

2.3. ΔC^* Calculations

Gruber et al. [1996] developed a method to estimate the total anthropogenic CO_2 inventory which has accumulated in the water column since preindustrial times. Although the details of the calculation are thoroughly discussed by Gruber et al., the basic concept of the calculation can be expressed in terms of the following equation:

$$C_{anth}\left(\frac{\mu mol}{kg}\right) = C_m - \Delta C_{bio} - C_{280} - \Delta C_{dis} \qquad (1)$$

where

C_{anth} anthropogenic carbon concentration;

C_m measured total carbon concentration;

ΔC_{bio} change in TCO_2 as a result of biological activity;

C_{280} TCO_2 of waters in equilibrium with an atmospheric CO_2 concentration of 280 µatm;

ΔC_{dis} air-sea difference in CO_2 concentration expressed in µmol kg^{-1} of TCO_2.

The Gruber et al. technique employs a new quasi-conservative tracer ΔC^*, which is defined as the difference between the measured TCO_2 concentration, corrected for biology, and the concentration these waters would have at the surface in equilibrium with a preindustrial atmosphere (i.e., $\Delta C^* = C_m - \Delta C_{bio} - C_{280}$). Rearranging (1) shows that ΔC^* reflects both the anthropogenic signal and the air-sea CO_2 difference (i.e., $\Delta C^* = C_{anth} + \Delta C_{dis}$). The air-sea disequilibrium component can then be discriminated from the anthropogenic signal using either information about the water age (e.g., from transient tracers such as CFCs or ^3H-^3He) or the distribution of ΔC^* in regions not affected by the anthropogenic transient. The details of this technique will not be covered here except as necessary to explain small modifications that were necessary for use with the WOCE Indian Ocean data set.

2.3.1. Preformed alkalinity equation. The first modification to the Gruber et al. [1996] technique involved a recalculation of the preformed alkalinity equation. The preformed alkalinity (Alk^0) of a subsurface water parcel is an estimate of the alkalinity that the water had when it was last at the surface. This value is necessary to determine the equilibrium concentration (C_{280}) of the waters. Gruber et al. generated a single global equation for estimating Alk^0 from salinity and the conservative tracer "PO" (PO = O_2+170*P) [Broecker, 1974] based on the data collected during GEOSECS, South Atlantic Ventilation Experiment, Transient Tracers in the Ocean/North Atlantic Study and Transient Tracers in the Ocean/Tropical Atlantic Study. Given the limited representation of the Indian Ocean in these data and the improved quality of today's measurements, the Gruber et al. fit was examined for a possible bias with respect to the WOCE/JGOFS results. Alk^0 values calculated from the Gruber et al. equation were found to be, on average, 7 ±12 µmol kg^{-1} lower than the WOCE/JGOFS measured surface alkalinity values. Rather than making assumptions about which parameters would provide the best fit to the surface alkalinity data, several possible parameters were tested based on previously noted correlations. Although salinity has been shown to generally correlate very strongly with surface alkalinity [Brewer et al., 1986; Millero et al., 1998b], some areas, such as the high-latitude regions, require additional parameters to fit regional changes in alkalinity. Some investigators have used temperature as an additional variable [e.g., Chen and Pytkowicz, 1979; Chen, 1990; Millero et al., 1998b]. Others, such as Gruber et al. [1996], have used other conservative tracers to compensate for the regional differences. The best fit for the WOCE/JGOFS, INDIGO, and CIVA Indian Ocean data, with pressures less than 60 dbars, is given by (2):

$$Alk^0 = 378.1 + 55.22 \times S + 0.0716 \times PO - 1.236 \times \theta \qquad (2)$$

Alk^0 has units of µmol kg^{-1} when salinity (S) is on the practical salinity scale, PO is in µmol kg^{-1}, and potential temperature (θ) is in degrees Celsius. The standard error in the new Alk^0 estimate is ±8.0

Table 1. Results From ANOVA Analysis of Alk^0 Fit.

	Coefficient	Standard Error	T Value	Pr(>ITI)
Intercept	378.1	8.9	42.2715	0.0000
Salinity	55.22	0.23	235.0369	0.0000
PO	0.0716	0.0041	17.4693	0.0000
Theta	-1.236	0.061	-20.3697	0.0000

The column labeled "Pr(>ITI)" gives the probability that the T value in the previous column is larger than the T table value in a student T test. Alk^0 is preformed alkalinity, an estimate of the alkalinity of a parcel of subsurface water when it was last at the surface.

µmol kg^{-1} based on 2250 data points. A standard ANOVA analysis of the fit shows that all four terms are highly significant (Table 1). Reevaluating the Alk^0 equation not only removed the 7 µmol kg^{-1} offset of Gruber's equation but also resulted in a 35% reduction in the uncertainty.

2.3.2. Denitrification Correction. A second modification to the original ΔC^* technique was necessary to properly account for the anoxic regions in the northern Indian Ocean. The C_{bio} term in (1) assumes that the remineralization of carbon in the interior of the ocean occurs in proportion to the oxygen uptake based on a standard Redfield type stoichiometry. The ratios used for these calculations were based on the global estimates of Anderson and Sarmiento [1994]. Gruber et al. [1996] demonstrated that the errors in the ΔC^* calculation due to uncertainties in the C:O stoichiometric ratio only become significant for AOU values greater than 80 µmol kg^{-1}. Given that most of the anthropogenic CO_2 is found in relatively shallow waters with low AOU, this error, on average, is small. For some regions of the Arabian Sea, however, oxygen depletion can be quite extensive at relatively shallow depths [Sen Gupta et al., 1976; Deuser et al., 1978; Naqvi and Sen Gupta, 1985]. In areas where the waters become anoxic, denitrification can significantly alter the dissolved carbon to oxygen ratio [Naqvi and Sen Gupta, 1985; Anderson and Dyrssen, 1994; Gruber and Sarmiento, 1997]. The dissolved carbon generated by denitrification shows up as high ΔC^* values as demonstrated at the northern end of the section in Figure 5a. The distribution of ΔC^* values along the density surface σ_θ=26.9-27.0 shows maximum values at both the northern and southern ends of the section. One would expect the uptake of anthropogenic CO_2 to generate the highest values close to the outcrop region in the south, but this surface does not outcrop in the north. Following the methods of Gruber and Sarmiento [1997], the denitrification signal can be estimated using the N* tracer. N* is a quasi-conservative tracer which can be used to identify nitrogen (N) excess or deficits relative to phosphorus (P). Using the global equation of Gruber and Sarmiento [1997], N* is defined as

$$N^*\left(\frac{\mu mol}{kg}\right) = 0.87(N - 16P + 2.90) \qquad (3)$$

Figure 5b shows the magnitude of the denitrification signal along the σ_θ=26.9-27.0 surface. The N* values were converted from nitrogen units to µmol C kg^{-1} based on a denitrification carbon to nitrogen ratio of 106:-104 [Gruber and Sarmiento, 1997]. Negative values reflect nitrogen fixation, while positive values indicate denitrification. As expected, the values of N* are essentially zero in the main Indian Ocean basin but show a strong denitrification signal at

middepths in the Arabian Sea. The low N* values at the north end of this surface (Figure 5b) are from the Bay of Bengal and show little or no denitrification in this region. Subtracting a denitrification correction term from the original ΔC* equation lowers the high ΔC* values at the northern end of the section leaving the expected maximum near the outcrop region (Figure 5c).

The final definition for ΔC* as used in this work is given by (4):

$$\Delta C^* = TCO_2^{(meas)} - TCO_2^{(S, T, Alk^0, 280)}$$
$$-\frac{117}{-170}(O_2 - O_2^{(sat)})$$
$$-\frac{1}{2}(TA - Alk^0 + \frac{16}{-170}(O_2 - O_2^{(sat)}))$$
$$-\frac{106}{-104}N^* \qquad (4)$$

where $TCO_2^{(meas)}$, TA, and O_2 are the measured concentrations for a given water sample in μmol kg^{-1}. Alk^0 is the preformed alkalinity value as described in section 2.3.1. $O_2^{(sat)}$ is the calculated oxygen saturation value that the waters would have if they were adiabatically raised to the surface. $TCO_2^{(S, T, Alk^0, 280)}$ is the TCO$_2$ value the waters would have at the surface with a TA value equal to Alk^0 and an fCO$_2$ value of 280 μatm.

2.3.3. Estimation of air-sea disequilibrium. To isolate the anthropogenic CO$_2$ component from ΔC*, the air-sea disequilibrium values (ΔC_{dis}) must be determined. *Gruber et al.* [1996] described two techniques for estimating these values on density surfaces. For deeper density surfaces one can assume that the waters far away from the outcrop region are free from anthropogenic CO$_2$. The mean ΔC* values in these regions therefore reflect only the disequilibrium value. For shallower surfaces the air-sea disequilibrium can be inferred from the ΔC^*_t tracer.

ΔC^*_t is the difference between C* and the concentration the waters would have in equilibrium with the atmosphere at the time they were last at the surface. The time since the waters were in contact with the surface is estimated from CFC-12 age (τ) and the atmospheric CO$_2$ concentration history as a function of time (fCO$_2\{t_{sample}-\tau\}$). The atmospheric CO$_2$ time history from 1750 through 1996 was determined from a spline fit to ice core and measured atmospheric values [*Neftel et al.*, 1994; *Keeling and Whorf*, 1996]. The CFC-12-based ages were determined following the technique described by *Warner et al.* [1996]. The apparent age of the water is determined by matching the CFC-12 partial pressure (pCFC-12) of the waters with the atmospheric CFC-12 concentration history (procedures and atmospheric time history provided by J. Bullister). Although CFCs do not give a perfect representation of the true calendar age of the waters, *Doney et al.* [1997] have shown that the CFC-12 and ^{3}H-^{3}He ages in the North Atlantic agree within 1.7 years for ages less than 30 years. *Gruber* [1998] successfully used both CFC and ^{3}H-^{3}He ages for his disequilibrium calculations in the Atlantic and has thoroughly discussed the assumptions and caveats associated with these techniques. The disequilibrium values on shallow density surfaces presented here were calculated using CFC-12 ages modified from the ΔC^*_t equation of *Gruber* [1998] to include the denitrification correction:

$$\Delta C^*_t = TCO_2^{(meas)} - TCO_2^{(S, T, Alk^0, fCO_2\{t_{sample}-\tau\})}$$
$$-\frac{117}{-170}(O_2 - O_2^{(sat)})$$
$$-\frac{1}{2}(TA - Alk^0 + \frac{16}{-170}(O_2 - O_2^{(sat)}))$$
$$-\frac{106}{-104}N^*$$

where $TCO_2^{(S, T, Alk^0, fCO_2\{t_{sample}-\tau\})}$ is the TCO$_2$ the waters would have at the surface with a TA value of Alk^0 and an fCO$_2$ value in equilibrium with the atmospheric CO$_2$ concentration at the time the waters were last at the surface (date of sample collection minus CFC age).

The CFC age method was used for waters with densities less than σ_θ = 27.25 and CFC-12 ages less than 40 years. The anthropogenic CO$_2$ of the waters with pressures less than 150 dbars or densities less than σ_θ = 25.95 was determined by subtracting the ΔC^*_t value estimated at each sample location from the corresponding ΔC* value. Given that the Indian Ocean does not extend into the high northern latitudes, the major outcrop region for Indian Ocean waters below the mixed layer is toward the south. Although other tracers might be used to identify multiple end-members, the CFC-12 ages on each density surface get steadily older toward the north, and the ΔC^*_t values are reasonably constant (see diamonds in Figure 6). This suggests that most of the water in the Indian Ocean is derived from the south or, at least in terms of the air-sea disequilibria, cannot be distinguished from other sources. The ΔC_{dis} term for the main Indian Ocean basin therefore was determined from a mean ΔC^*_t value on each surface. The mean ΔC_{dis} terms were then subtracted from the individual ΔC* values to determine the anthropogenic component. Table 2 summarizes the ΔC_{dis} values for the density surfaces estimated exclusively from the ΔC^*_t method.

One major exception to the southern source waters is observed in the Arabian Sea. Although none of the surfaces with σ_θ values greater than 26.0 outcrop in the Arabian Sea, a number of higher-density surfaces do outcrop in the Red Sea and Persian Gulf. These outcrops could provide pathways for the introduction of CFCs and anthropogenic CO$_2$ into the northern Arabian Sea and could reset the disequilibria term. *Wyrtki* [1973] noted that the Red Sea and Persian Gulf waters mix in the Arabian Sea to form the high-salinity North Indian Intermediate Water (NIIW). The ΔC^*_t values in the Arabian Sea do vary significantly and generally have a strong correlation with salinity. The CFC-12 ages also begin to get younger toward the northern end of the Arabian Sea. These high-salinity waters appear to have a higher disequilibria term than the lower-salinity waters that make up the majority of the Indian Ocean intermediate waters.

To account for this phenomenon, the Arabian Sea waters (north of 5°N and west of 78°E) were isolated, and the ΔC^*_t values were fit against salinity with a linear regression. Thus this region was treated as a two-end-member mixing scenario between the high-salinity NIIW and the lower-salinity waters of the main Indian Ocean basin. The ΔC_{dis} values in this region were determined based on the relative contributions of the two end-members using salinity as a conservative tracer. The coefficients for the Arabian Sea fits are given in Table 2. The difference between the high-salinity and lower-salinity disequilibria generally decreased as densities increased (note decreasing slope values in Table 2) to the point where the Arabian Sea disequilibria values were no longer distinguishable from the main Indian Ocean basin values. The additional terms were dropped for surfaces where the two end-member mixing terms resulted in values within the error of the basin-wide mean (Table 2).

As stated previously, the disequilibria term for the deeper, CFC free surfaces was determined directly from the mean ΔC* value of each density interval. Careful examination of the extent of CFC penetration along the density surface was used to limit data used in
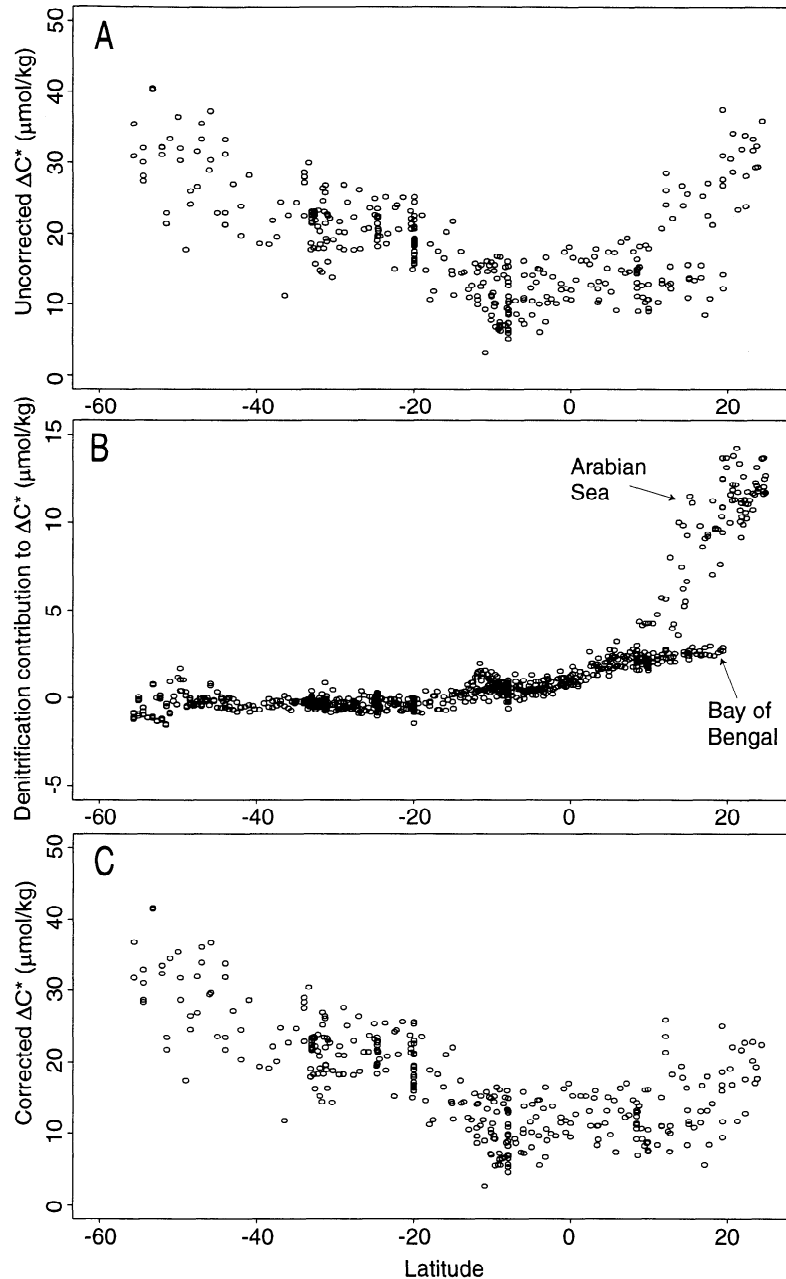
Figure 5. ΔC^* values for data on the 26.9 - 27.0 σ_θ surface: (a) calculated without denitrification, (b) denitrification signal put in terms of ΔC^*, (c) with denitrification correction (i.e., data in Figure 5a minus the data in Figure 5b).

determining the ΔC_{dis} term. Only regions where CFC concentrations were below a reasonable blank (0.005 pmol kg⁻¹) were considered. The ΔC_{dis} values determined using this method are summarized in the lower half of Table 3 ($\sigma_\theta > 27.5$).

Determination of the ΔC_{dis} values for either shallow or deep surfaces is relatively straightforward using the techniques mentioned above. It is not straightforward, however, to estimate the ΔC_{dis} values for intermediate levels where the CFC ages are relatively old and may be significantly influenced by mixing and yet the waters could have enough anthropogenic CO₂ to influence the

estimates based on ΔC^*. The effect of using the ΔC^* technique in waters that actually have anthropogenic CO₂ would be to overestimate the ΔC_{dis} term and thus underestimate the anthropogenic CO₂. The effect of mixing on the CFC ages, however, generally results in an underestimation of the CFC age which would lead to an underestimation of the ΔC_{dis} term and an overestimation of the anthropogenic CO₂. The CFC age technique has additional problems in waters with σ_θ values greater than 27.25, because the waters with the younger ages are all found in the very high latitudes of the Southern Ocean and generally are not directly venti-

Table 2. Values of ΔC_{dis} Determined on Potential Density (σ_θ) Intervals

Potential Density Range	Main Basin Mean (SDM)	Main Basin Number of Points	Arabian Intercept (SD)	Arabian Slope (SD)	Arabian Number of Points
25.95-26.05	-1.3 (±0.88)	56	-740 (±92)	21.3 (±3)	12
26.05-26.15	-0.7 (±1.21)	42	-745 (±130)	21.4 (±4)	12
26.15-26.25	-3.4 (±0.65)	63	-699 (±76)	20.0 (±2)	11
26.25-26.35	-4.8 (±0.62)	61	-516 (±90)	14.8 (±3)	12
26.35-26.45	-5.6 (±0.48)	83	-316 (±84)	9.1 (±2)	20
26.45-26.55	-7.1 (±0.34)	103	-558 (±87)	15.9 (±2)	21
26.55-26.65	-7.2 (±0.32)	123	-512 (±53)	14.5 (±1)	28
26.65-26.75	-8.9 (±0.27)	152	-397 (±52)	11.2 (±1)	34
26.75-26.85	-9.1 (±0.23)	254	-428 (±66)	12.0 (±2)	28
26.85-26.95	-11.2 (±0.31)	209	-285 (±115)	7.9 (±3)	6
26.95-27.00	-12.2 (±0.35)	104	-	-	-
27.00-27.05	-13.8 (±0.48)	92	-	-	-
27.05-27.10	-15.2 (±0.40)	90	-	-	-
27.10-27.15	-16.3 (±0.47)	84	-	-	-
27.15-27.20	-17.1 (±0.51)	89	-	-	-
27.20-27.25	-19.5 (±0.56)	74	-	-	-

Standard deviations (SD) are given for the slope and intercept terms for the Arabian Sea data. Standard deviation of the mean (SDM, i.e., standard deviation weighted by the number of individual determinations) is given for each main basin estimate. Values of ΔC_{dis} are given in μmol kg^{-1}. Dashes indicate value not determined.

lated in these regions. Therefore the basic assumption that the ΔC_{dis} term can be determined by following the density level to its outcrop and examining the younger waters there is not valid.

As a general rule, the errors associated with the CFC age technique increase at higher density levels, and the errors associated

with the ΔC^* technique decrease at higher density levels. To minimize the errors in the final ΔC_{dis} determination, waters with σ_θ values between 27.25 and 27.5 were evaluated using a combination of the two methods mentioned above. The 27.25 cut in the CFC age technique was chosen because this density corresponds

Table 3. Values of ΔC_{dis} Determined on Potential Density (σ_θ) Intervals

Potential Density Range	Mean ΔC^* (SDM)	Number of Points	Mean ΔC^*_t (SDM)	Number of Points	Final Mean ΔC_{dis} (SDM)
27.25-27.30	-2.3 (±0.45)	42	-19.7 (±0.98)	22	-8.3 (±1.13)
27.30-27.35	-4.0 (±0.49)	45	-21.0 (±0.84)	19	-9.1 (±1.06)
27.35-27.40	-5.3 (±0.44)	72	-22.5 (±1.25)	7	-6.8 (±0.69)
27.40-27.45	-7.1 (±0.26)	92	-23.5 (±0.83)	10	-8.7 (±0.54)
27.45-27.50	-7.9 (±0.30)	98	-25.0 (±1.65)	7	-9.0 (±0.51)
27.50-27.55	-9.3 (±0.28)	93	-	-	-9.3 (±0.28)
27.55-27.60	-10.7 (±0.28)	92	-	-	-10.7 (±0.28)
27.60-27.65	-11.3 (±0.34)	125	-	-	-11.3 (±0.34)
27.65-27.70	-13.0 (±0.36)	127	-	-	-13.0 (±0.36)
27.70-27.75	-14.8 (±0.30)	184	-	-	-14.8 (±0.30)
27.75-27.80	-15.3 (±0.24)	349	-	-	-15.3 (±0.24)
>27.80	-18.6 (±0.15)	629	-	-	-18.6 (±0.15)

Standard deviation of the mean given in brackets (SDM, i.e., standard deviation weighted by the number of individual determinations).Values of ΔC_{dis} are given in μmol kg^{-1}. Dashes indicate value not determined.

with the core of the Antarctic Intermediate water and also gener-ally the highest-density water that outcrops in this region [*Wyrtki*, 1973; *Levitus and Boyer*, 1994; *Levitus et al.*, 1994]. To help ensure that the ΔC_{dis} values were determined on waters moving into the main Indian Ocean basin, mean ΔC^*_t values were only estimated from samples north of 35°S with CFC-12 ages less than 40 years. Mean ΔC^* values were also determined on the same den-sity surfaces for samples where CFCs were measured, but concen-trations were below 0.005 pmol kg^{-1}. The final mean value used for the ΔC_{dis} correction on each surface was determined from the mean of the combined individual estimates from each method (Table 3).

Examination of the individual and combined means in Table 3 indicates that there is a sizeable spread in the estimates from the two techniques in the overlap region. This difference is maximized since these density levels are pushing the limits of both techniques, and the errors in both estimates serve to increase this difference. Since the number of points available from the CFC age technique generally decreased at greater density levels and the number of points from the ΔC^* technique generally increased at greater den-sity levels, the mean becomes progressively more heavily weighted toward the ΔC^* technique as the density levels increased. Although this is not the ideal solution, we believe that this mini-mizes the potential errors as much as possible. The technique used to estimate final ΔC_{dis} values in this region could systematically bias the anthropogenic CO$_2$ inventory estimates. The magnitude of this potential error on the final inventory was estimated to be approximately ±1.8 Pg C by integrating the difference between the two methods over the effected water volume. This estimate repre-sents a maximum potential error since the known limitations of each method work to increase the differences in ΔC_{dis}.

2.3.4. Time adjustment for INDIGO data. One difficulty with combining data from different cruises for a time-dependent calculation like the anthropogenic CO$_2$ inventory is the issue of getting the data sets referenced to a common time. One of the advantages of the WOCE/JGOFS Indian Ocean survey data is the fact that all of the samples were collected in a little over a year's time. In terms of the CO$_2$ inventory this is essentially a synoptic data set. The couple of years between the CIVA1 cruise and the WOCE/JGOFS data are also not distinguishable in terms of the anthropogenic increase. The INDIGO data, however, were col-lected 8-10 years before the WOCE/JGOFS data set and must be adjusted to reflect the anthropogenic uptake during that time. Unfortunately, any correction of this sort can have large errors and potentially bias the results. This problem must be weighed against the errors of ignoring the time difference between cruises or omit-ting these data entirely. The decision to correct the INDIGO data was based on two factors. First, analysis of the change in anthropo-genic inventory between GEOSECS and WOCE (discussed below) indicated that a significant fraction of the total anthropogenic uptake has occurred in the past 2 decades. Second, careful exami-nation of objective maps of anthropogenic CO$_2$ made prior to the INDIGO correction showed obvious, anomalously low concentra-tions in the regions strongly dependent on the INDIGO data. Two different adjustment functions were made depending on whether the stations were located in the main Indian Ocean basin or in the Southern Ocean.

North of 30°S, where portions of the INDIGO data were located relatively near WOCE stations, a crossover comparison of the INDIGO anthropogenic CO$_2$ concentrations as a function of

density was made with the WOCE/JGOFS data in that region. The difference between the two data sets was evaluated at σ_θ intervals of 0.05 from the surface to $\sigma_\theta = 27.5$ and added to the INDIGO data. This correction ranged from approximately 12 μmol kg^{-1} at the surface down to zero at 27.5.

South of 30°S, there were very few WOCE or CIVA1 stations close enough for a proper crossover comparison. It was clear from the northern data, however, that some correction was necessary. Given that the isolines for most properties in the Southern Ocean run east-west, we decided to correct the southern INDIGO data based on a crossover comparison with all results from CIVA1 and WOCE cruises in that region. The average adjustment for the southern stations was approximately 11 μmol kg^{-1} over the same density range. The magnitude of the corrections in both regions is consistent with the expected increase over the time period between cruises.

2.3.5. Evaluation of Errors. Error evaluation is much more difficult for the ΔC^* method than for the time series approach because of potential systematic errors associated with some of the parameters (i.e., the biological correction). The random errors associated with the anthropogenic CO$_2$ can be determined by prop-agating through the precision of the various measurements required for the calculation of (4).

$$\{\sigma_{C_{anth}}\}^2 = \{\sigma_C\}^2 + \{-\sigma_{C_{eq}}\}^2$$

$$+ \{(-R_{CO} - 0.5R_{NO})\sigma_{O_2}\}^2$$

$$+ \{(R_{CO} + 0.5R_{NO})\sigma_{O_{2[sat]}}\}^2$$

$$+ \{-0.5\sigma_{TA}\}^2 + \left\{(-\frac{\partial C_{eq}}{\partial TA} + 0.5)\sigma_{Alk^0}\right\}^2$$

$$+ \{0.8667\sigma_N\}^2 + \{13.867\sigma_P\}^2$$

$$+ \left\{0.8667(-P - \frac{N - 16P + 2.9}{120})\sigma_{R_{N:P[nitr]}}\right\}^2$$

$$+ \{-0.00111(N - 16P + 2.9)\sigma_{R_{N:P[denitr]}}\}^2$$

$$- \{\sigma_{\Delta C_{dis}}\}^2 \qquad (6)$$

where $\sigma_C = 2$ μmol kg^{-1}; $\sigma_{C_{eq}} = 4$ μmol kg^{-1}; $\sigma_{O_2} = 1$ μmol kg^{-1}; $\sigma_{O_{2[sat]}} = 4$ μmol kg^{-1}; $\sigma_{TA} = 4$ μmol kg^{-1}; $\frac{\partial C_{eq}}{\partial TA} = 0.842$; $\sigma_{Alk^0} = 7.8$ μmol kg^{-1}; $\sigma_N = 0.2$ μmol kg^{-1}; $\sigma_P = 0.02$ μmol kg^{-1}; $\sigma_{R_{N:P[nitr]}} = 0.25$; and $\sigma_{R_{N:P[denitr]}} = 15$. The equation for the random error analysis is adapted from *Gruber et al.* [1996] (exclud-ing those terms that involve the C:O Redfield error) with additional terms for the error propagation of the N* correction [*Gruber and Sarmiento*, 1997]. The terms involving the C:O are evaluated sepa-rately below because the random errors cannot be isolated from po-tential systematic errors. The sigma values used in (6) were either taken from the appropriate WOCE cruise reports or from previously determined estimates of *Gruber et al.* [1996] and *Gruber and*

Sarmiento [1997]. The error in the ΔC_{dis} term is taken from the average value for the standard deviation of the mean for the examined surfaces ($\sigma_{\Delta C_{dis}}$ = 0.5 μmol kg^{-1}). The formulation given in (6) results in an estimated error of 6.1 μmol kg^{-1}. This estimate is larger than the standard deviation of the ΔC^* values below the deepest anthropogenic CO_2 penetration depth (±2.8 μmol kg^{-1} for pressure > 2000 dbars) suggesting that the propagated errors may be a maximum estimate of the random variability.

The potential systematic errors associated with the anthropogenic CO_2 calculation are much more difficult to evaluate. The random error estimate above includes all terms except those associated with the C:O biological correction. Although other terms involving N:O and N:P corrections potentially have systematic offsets associated with errors in the ratio estimates, the only potentially significant errors involve the C:O corrections [*Gruber et al.*, 1996; *Gruber*, 1998].

There is evidence, however, that the *Anderson and Sarmiento* [1994] stoichiometric ratios must be reasonably close to the actual remineralization ratios observed in the Indian Ocean. Figure 6 is a plot of ΔC^*_t based on CFC-12 ages for the density interval from σ_θ = 27.1 to σ_θ = 27.15. The diamonds are the values calculated from (5). These values represent the preserved air-sea disequilibrium value for the past 40 years and should be constant if the air-sea dis-

equilibrium has not changed over time (i.e., that the surface ocean CO_2 is increasing at the same rate at the atmosphere). A linear regression of the diamonds in Figure 6 yields a slope that is not significantly different from zero. The circles and pluses are the ΔC^*_t values one would get by using a C:O ratio of -0.60 and -0.78 in (5), respectively. These C:O values represent one standard deviation from the *Anderson and Sarmiento* [1994] mean value of -0.69. The -0.60 ratio results in values with a significant positive slope. This slope would imply that the surface ocean CO_2 is increasing much slower than the atmospheric increase. While this is possible, the -0.60 ratio is much larger than historical Redfield estimates and would be very difficult to justify. The -0.78 ratio is more typical of historical estimates but results in a significant negative slope in the ΔC^*_t values with time. A negative slope would imply that carbon is accumulating in the ocean faster than the atmosphere. Neither of these scenarios seems very likely. The fact that none of the ΔC^*_t values on the examined surfaces exhibit a statistically significant slope suggests that the C:O value of -0.69 does accurately represent the remineralization ratio for these waters and supports the methodology of taking a mean value of ΔC^*_t on these density surfaces.

A sensitivity study was also used to evaluate the potential error associated with an incorrect C:O value. Two additional estimates of anthropogenic CO_2 were determined using the -0.60 and -0.78
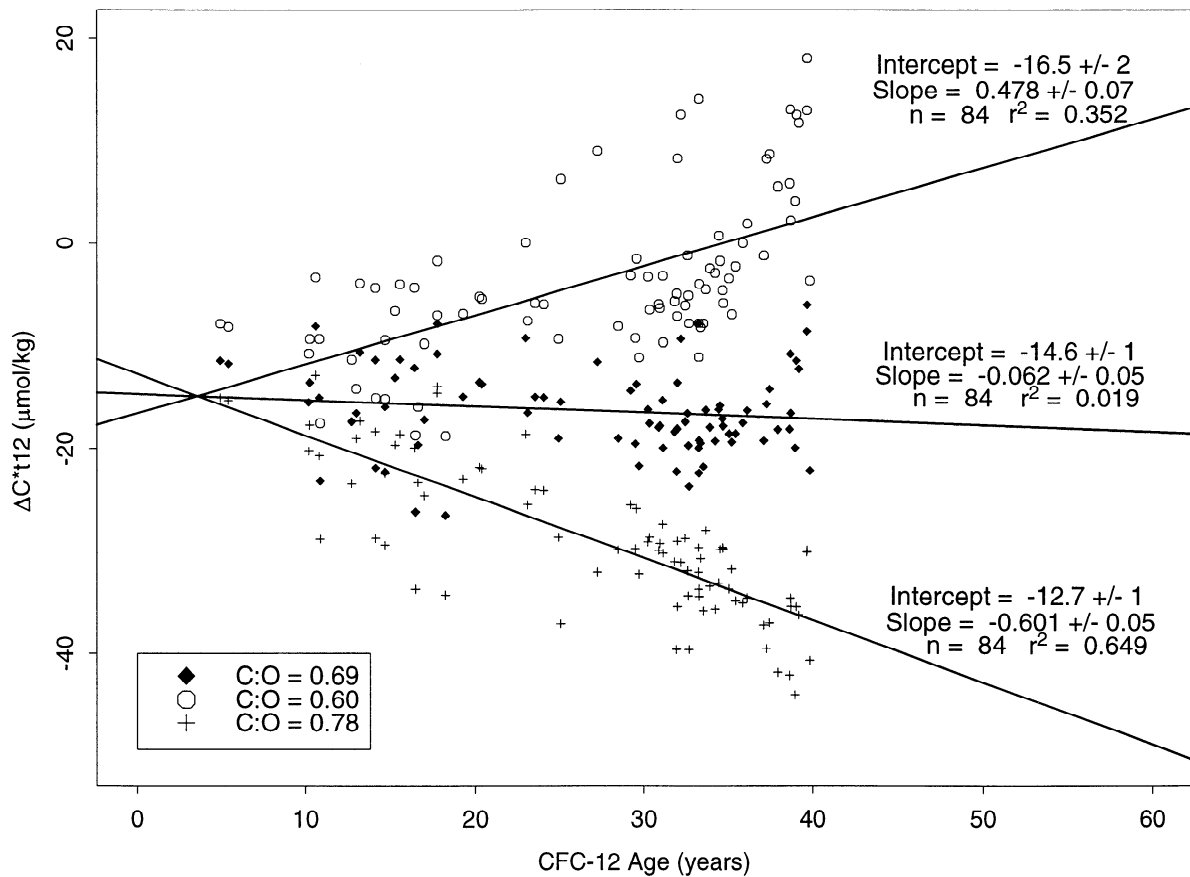

Figure 6. Plot of ΔC^*_t based on CFC-12 ages for the density interval from σ_θ = 27.1 to 27.15 versus CFC-12 age. The diamonds were calculated using the *Anderson and Sarmiento* [1994] C:O (-0.69). The circles and pluses were calculated from C:O of -0.60 and -0.78, respectively. Lines and text give results from a linear regression of the three sets of data.

C:O values. Since the C:O correction applies to both ΔC^* and the ΔC^*_t terms, the disequilibrium values were reevaluated in the same manner as described above. The range of anthropogenic values from these three estimates varied as a function of apparent oxygen utilization (AOU) from 0.0 to 22 with an average difference of only 4.2 μmol kg^{-1}. Because the C:O correction affects both the ΔC^* and ΔC^*_t terms together, much of the systematic error in the final anthropogenic estimate ($\Delta C^*-\Delta C^*_t$) cancels out.

2.4. Inventory Estimates

Basin-wide anthropogenic and excess CO_2 concentrations (WOCE/JGOFS - GEOSECS) were evaluated on a 1° grid at 100 m intervals between the surface and 2600 m using the objective mapping techniques of *Sarmiento et al.* [1982]. Total anthropogenic CO_2 was mapped over an area from 20° to 120°E and 70°S to 30°N (excluding areas of land, the Red Sea, the Persian Gulf, and the South China Sea). Because the WOCE/JGOFS data set did not cover much of the Southern Ocean, the excess CO_2 maps were limited to the area north of 35°S. The values at each level were multiplied by the volume of water in the 100 m slab and summed to generate the total anthropogenic or excess CO_2 inventory. The method of integrating mapped surfaces compared very well with the technique of vertically integrating each station and mapping the station integrals.

It is extremely difficult to evaluate a reasonable estimate of the potential errors associated with the inventory estimates. A simple propagation of errors implies that the random errors associated with any individual anthropogenic estimate is approximately ±6.1 μmol kg^{-1}, but these errors should essentially cancel out for an integrated inventory based on nearly 25,000 individual estimates. Systematic errors have by far the largest impact on the inventory estimates. Potential errors as large as ±1.8 Pg C have been estimated for the ΔC_{dis} term. Sensitivity studies with the C:O variations give a range of total inventory estimates of ±2.5 Pg C. Other systematic errors could also be generated from the denitrification term, the terms involving N:O, the time correction for the INDIGO data, and the mapping routines used in the inventory estimates. The magnitude of these errors is believed to be much smaller than the uncertainty in either the C:O correction or the ΔC_{dis} determination. Propagation of the two estimated uncertainties gives an overall error of approximately ±3 Pg C for the total inventory. An error of roughly 15% is comparable to previous error estimates using this technique [*Gruber et al.*, 1996; *Gruber*, 1998]. Errors for regional inventories are assumed to scale to the total.

3. Results and Discussion

The excess CO_2 concentrations for the Indian Ocean range from 0 to 25 μmol kg^{-1}. The most prominent feature in the excess CO_2 distribution, as shown with representative sections in the eastern and western Indian Ocean (Figure 7), is the maximum in concentrations at midlatitudes (~ 40°S). This maximum is coincident with the relatively strong gradient in surface density associated with the Subtropical Convergence and the transition from the high-salinity subtropical gyre waters to the low-salinity Antarctic waters. The outcropping of these density surfaces and subsequent sinking of surface waters provides a pathway for excess CO_2 to enter the interior of the ocean. Relatively high excess CO_2 concentrations can also be observed at the very northern end of the western section (Figure 7a). Although not readily evident from this

section, the distribution of concentration gradients indicates that excess CO_2 is entering the northern Indian Ocean from the Persian Gulf and Red Sea regions. This is likely to result from the outcropping of density surfaces in these areas which are not ventilated in the main Indian Ocean basin. The implied Red Sea and Persian Gulf sources of CO_2 are consistent with uptake estimates of anthropogenic CO_2 in these areas as observed by *Papaud and Poisson* [1986]. The third major feature observed in the excess CO_2 distribution is a dramatic shoaling of the excess CO_2 isolines south of approximately 40°S. *Poisson and Chen* [1987] attributed the low anthropogenic CO_2 concentrations in Antarctic Bottom Water to a combination of the pack sea ice blocking air-sea gas exchange and the upwelling of old Weddell Deep Water. This explanation is consistent with the observed excess CO_2 distributions in this study.

The general features observed with excess CO_2 are also observed in the anthropogenic CO_2 distribution (Figure 8). The range of values, however, extends up to 55 μmol kg^{-1}. The maximum depth of the 5 μmol kg^{-1} contour is approximately 1300 m at around 40°S, only 200 m deeper than the maximum depth of the 5 μmol kg^{-1} contour of excess CO_2. The similarity in maximum penetration depth between the 200 year and the 18 year anthropogenic CO_2 accumulation, together with the wide range of depths covered by the 5 μmol kg^{-1} isoline, indicates that the primary pathway for CO_2 to enter the ocean's interior is from movement along isopycnals, not simple diffusion or cross isopycnal mixing from the surface. The 1300 m penetration results from the downwarping of the isopycnals in the region of the Subtropical Convergence. Likewise, the low anthropogenic CO_2 concentrations in the high-latitude Southern Ocean result from the compression and shoaling of isopycnal surfaces in that region. Although the complex oceanography of the Southern Ocean may call into question some of the assumptions regarding mixing and nutrient uptake ratios with these techniques, both the time series excess CO_2 and the ΔC^* anthropogenic CO_2 calculations clearly indicate that the anthropogenic CO_2 concentrations south of approximately 50°S are relatively small.

The distribution of anthropogenic CO_2 determined in this study is similar to the distribution presented by *Chen and Chen* [1989] based on GEOSECS and INDIGO data. Although the penetration depth at 40°S was slightly deeper than observed with this study (1400-1600 m for the 5 μmol kg^{-1} isoline), Chen and Chen also observed a significant shoaling of the anthropogenic CO_2 isolines toward the south. They suggest that anthropogenic CO_2 has only penetrated a few hundred meters into the high-latitude (>50°S) Southern Ocean.

There has been debate in the literature over recent years as to the importance of the Southern Ocean as a sink for anthropogenic CO_2 [e.g., *Sarmiento and Sundquist*, 1992; *Keeling et al.*, 1989; *Tans et al.*, 1990]. Most of the recent data-based estimates, however, indicate a relatively small Southern Ocean sink [*Poisson and Chen*, 1987; *Murphy et al.*, 1991; *Gruber*, 1998; this study]. The lack of observed anthropogenic CO_2 in the Southern Ocean is also qualitatively consistent with $\Delta^{14}C$ estimates which show no measurable storage of bomb ^{14}C in the Southern Ocean since GEOSECS [*Leboucher et al.*, 1998; R. Key, unpublished data, 1998]. Recent studies by *Bullister et al.* [1998], which show evidence of deep CFC penetration in the Southern Ocean, may appear to contradict these low anthropogenic CO_2 estimates, but we believe it is further evidence that one must be careful when inferring anthropogenic carbon distributions from other tracers. One possible explanation of this apparent discrepancy may be the CFC equilibration
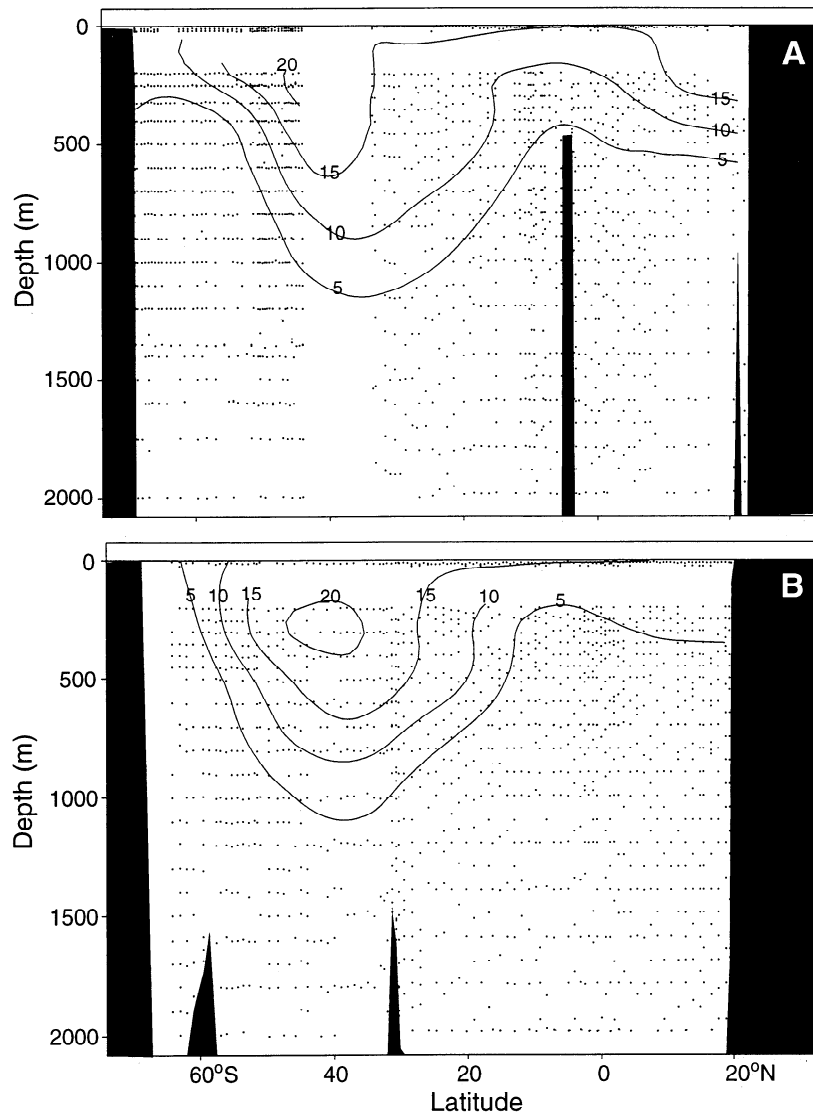
Figure 7. Sections of excess CO$_2$ along (a) ~57°E and (b) ~92°E. Dots indicate sample locations used in sections. Note that I6S data along 30°E were brought into the line of section for contours south of 40°S in Figure 7a.

rate of days which is significantly faster than the CO$_2$ equilibration time of months [e.g., *England*, 1995; *Warner and Weiss*, 1985; *Tans et al.*, 1990]. This can become an issue in the Southern Ocean where upwelling and convection may allow the CFCs to equilibrate to a greater extent than the CO$_2$. Again, we acknowledge the limitations of the methods used in the Southern Ocean, and it is possible that the apparent discrepancy in the CFC penetration versus the CO$_2$ penetration may also be an issue of detection limits. With a detection limit that is approximately 6 μmol kg^{-1}, it is not possible to say with this technique that the concentration of anthropogenic CO$_2$ below 500 m at 60°S is zero. However, we can say with some confidence that the concentration is not 10 μmol kg^{-1} or greater. Since there is no natural oceanic source of CFCs and these compounds are not biologically utilized, the ability to detect them is much greater. If mixing has diluted the anthropogenic signal to concentrations just below detection limits, it is possible that carbon measurement based techniques would underestimate the Southern Ocean sink.

The total anthropogenic CO$_2$ inventory for the main Indian Ocean basin (north of 35°S) was 13.6±2 Pg C in 1995. The increase in CO$_2$ inventory since GEOSECS was 4.1±1 Pg C for the same area. This represents a nearly 30% increase in the past 18 years relative to the total accumulation since preindustrial times. The relative oceanic increase is very similar to the 31% increase observed in atmospheric concentrations over the same time period [*Keeling and Whorf*, 1996]. This similarity suggests that the oceans, at least for now, are keeping pace with the rise in atmospheric CO$_2$. Approximately 6.7±1 Pg C are stored in the Indian sector of the Southern Ocean giving a total Indian Ocean inventory (between 20° and 120°E) of 20.3±3 Pg C in 1995.

To put these results in a global perspective, the total inventory for the Indian Ocean is only half that of the Atlantic (40±6 Pg C [*Gruber*, 1998]), but it contains an ocean volume that is nearly 80% of the Atlantic. The main difference between the two oceans, of course, is that the Indian Ocean does not have the high northern latitude sink that the Atlantic has. The big unknown at this point is

the anthropogenic inventory of the Pacific. With nearly 50% of the total ocean volume the Pacific has the potential to be the largest oceanic reservoir for anthropogenic CO_2.

4. Comparison With Princeton Ocean Biogeochemistry Model

Current IPCC anthropogenic estimates are primarily based on global carbon models. Ultimately, these models are necessary to predict the oceanic response to future climate scenarios. It is important, however, to validate these models. One way to compare results is to examine profiles of the average anthropogenic concentrations such as those shown in Figure 9. The model presented here is the Princeton Ocean Biogeochemistry Model (OBM). The Princeton OBM is based on the circulation of *Toggweiler et al.* [1989] with explicit parameterization for the biological and solubility carbon pumps [*Sarmiento et al.,* 1995; *Murnane et al.,* 1998]. On this scale the model-based concentrations for both the total anthropo-

genic CO_2 and the increase since GEOSECS appear to be reasonably consistent with the data. The primary difference is slightly higher values at middepths in the data-based estimates. A more detailed examination, however, indicates that the regional distribution of the model-based estimates is significantly different than the data-based distribution. Figure 10 presents maps of the vertically integrated excess CO_2 normalized to a unit area. The model shows a consistent decrease in column inventory toward the north. The lowest inventories in the data-based map are in a narrow band just south of the equator. The highest values are found in the southeastern Indian Ocean. Relatively high values are also observed in the Arabian Sea in the regions near the Red Sea and the Persian Gulf. The small patch of lower values immediately outside the Gulf of Aden does not result from low concentrations but rather results from the shallow water depth associated with the mid-ocean ridge in that area. The low values east of there, however, do result from lower concentrations near the southern tip of India. The total model-based inventory for the region north of 35°S is approximately 0.61 times the data-based inventory (Table 4).
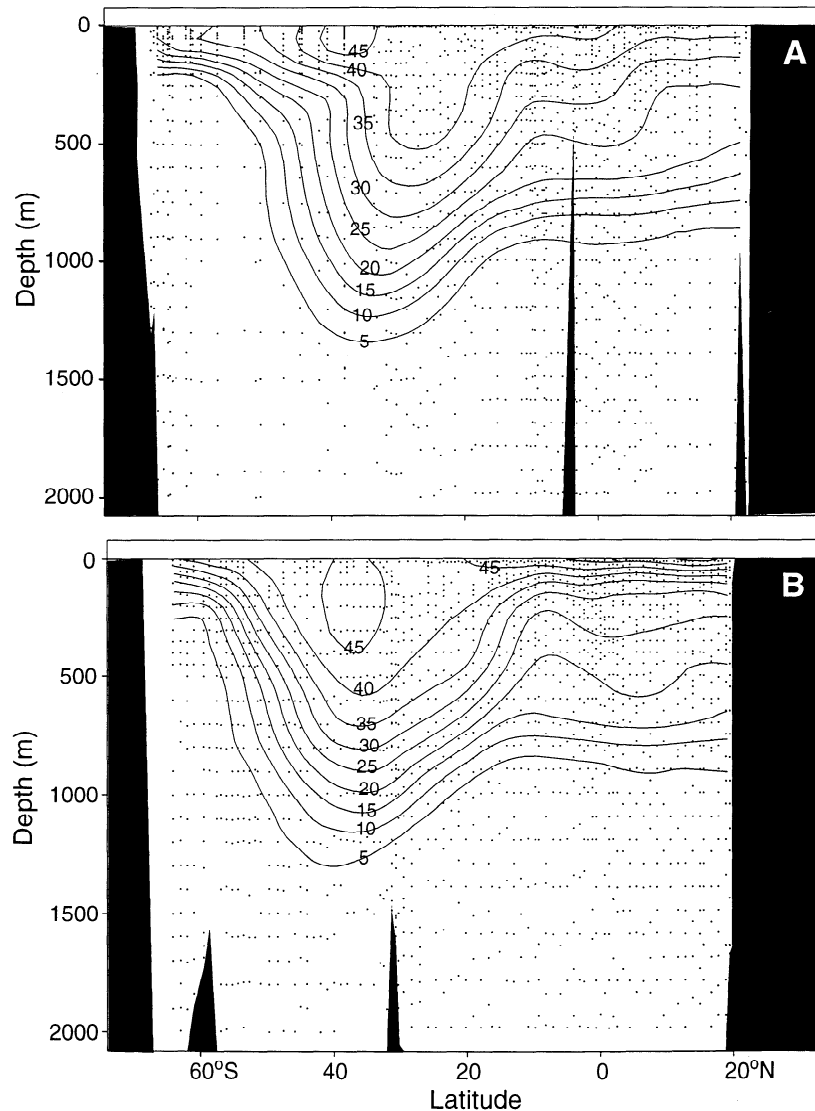

Figure 8. Sections of anthropogenic CO_2 along (a) ~57°E and (b) ~92°E. Dots indicate sample locations used in sections.
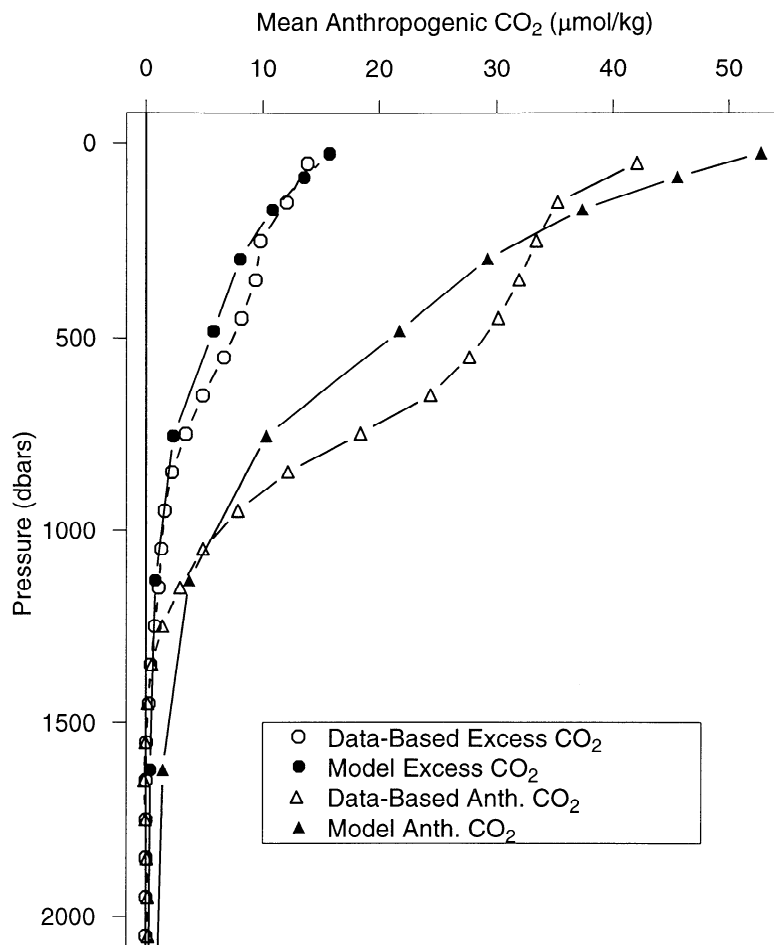
Figure 9. Profile of area weighted mean anthropogenic CO_2 concentrations for model (solid symbols) and data-based (open symbols) estimates for main Indian Ocean basin (north of 35°S). Circles show increase since GEOSECS (1978-1995). Triangles show total increase since preindustrial times.

Figure 11 shows maps of total anthropogenic CO_2 column inventory. As with the excess CO_2, the model predicts decreasing anthropogenic concentrations north of 35°S. The data-based distribution pattern is similar to the data-based excess CO_2 pattern with a minimum inventory band south of the equator and higher values toward the north and south. Similar to the findings with excess CO_2, the model-based anthropogenic inventory north of 35°S is approximately 0.68 times the data-based inventory (Table 4). The largest difference between the data-based results and the model is evident, however, in the Southern Ocean (south of 35°S). In this region the model anthropogenic inventory is nearly 2.6 times the data-based inventory (Table 4). The primary reason for this difference is the presence of a large convective cell in the model at approximately 55°S and 90°E in the Southern Ocean. This is a region of intense, unrealistic convection which pumps relatively high concentrations of anthropogenic CO_2 down in excess of 4000 m. This problem is a known shortcoming with the mixing scheme used in several GCMs [e.g., England, 1995] but has never before been quantified in terms of its direct effect on anthropogenic CO_2 storage by the models. It is beyond the scope of this paper to examine the details of the model physics; however, this same general trend of getting too much anthropogenic CO_2 into the Southern Ocean has been observed in comparisons with three other global

carbon models with a range of mixing and advective schemes [C. Sabine, unpublished results, 1998]. This cursory comparison with the Princeton OBM clearly demonstrates the diagnostic usefulness of comparing the data distributions with models.

5. Conclusions

Although the general techniques proposed by Gruber et al. [1996] and Wallace [1995] can be important tools for estimating global anthropogenic CO_2, careful consideration must be used when applying these techniques to new regions. Complicating factors such as those found in the Arabian Sea can influence the quality of the estimates if not properly addressed. An additional term had to be added to the basic ΔC^* calculation to account for denitrification in the Arabian basin. For the excess CO_2 calculations a categorical variable was used to remove regional biases in the GEOSECS fit.

With the above mentioned modifications the anthropogenic inventory of the Indian Ocean was shown to be relatively small, approximately half of that found in the Atlantic. This study provides an important baseline for future studies of the Indian Ocean. The calculations presented here suggest that the oceanic increase in carbon storage (30%) has roughly kept pace with the atmo-
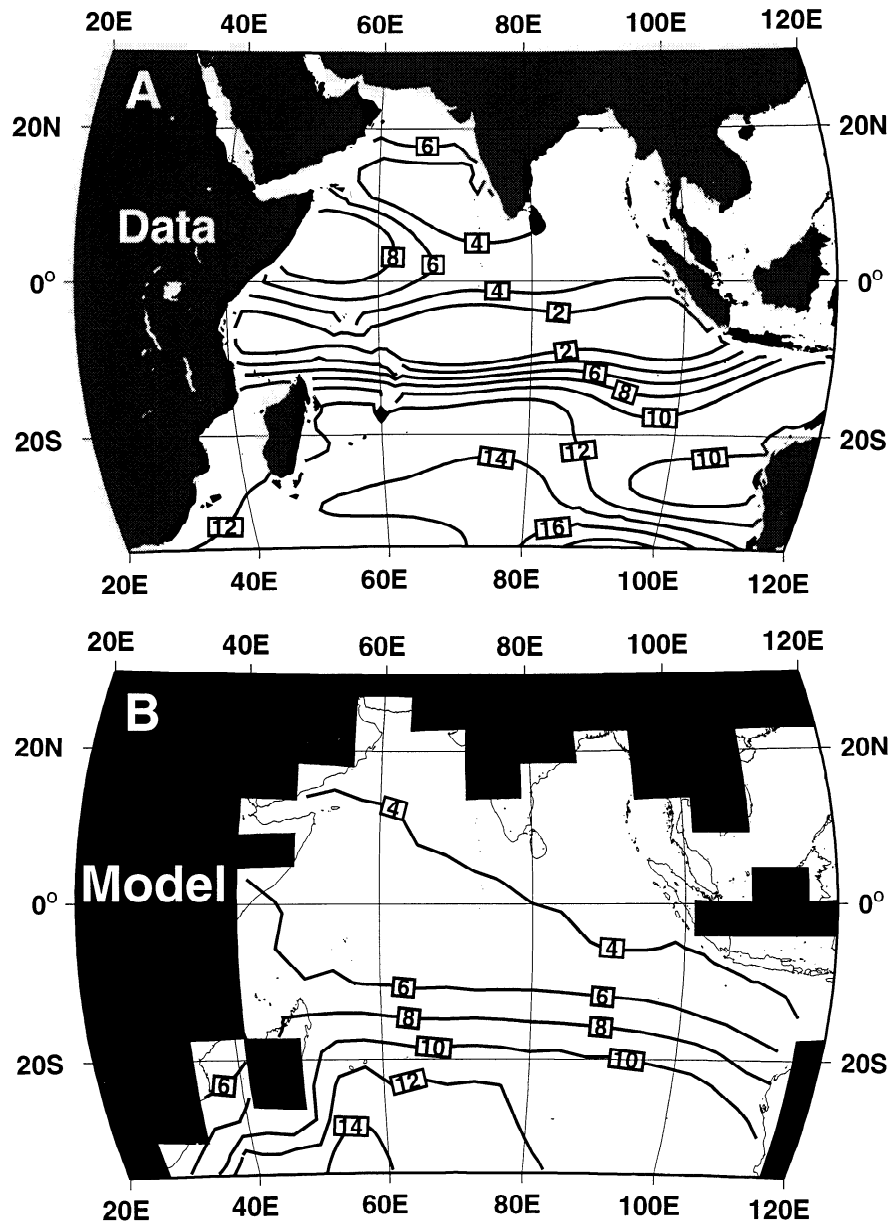
Figure 10. Maps of vertically integrated excess CO$_2$ based on (a) data and (b) model estimates. Contours are in mol m^{-2}. Solid regions indicate land mask used for inventory estimates. Thin lines in Figure 10b indicate land regions used in Figure 10a.

Table 4. Summary of Data Based and Model Based Inventory Estimates

	Total Anthropogenic CO$_2$,$^\alpha$ Pg C	Southern Ocean Anthropogenic CO$_2$,$^\beta$ Pg C	Main Basin Anthropogenic CO$_2$,$^\chi$ Pg C	Main Basin Excess CO$_2$,$^\chi$ Pg C	Increase since GEOSECS, %
Data based	20.3±3	6.7±1	13.6±2	4.1±1	29.9
Model based	26.7	17.4	9.3	2.5	26.7

$^\alpha$Area between 20°-120°E.
$^\beta$Latitude is < 35°S.
$^\chi$Latitude is > 35°S.

spheric increase (31%) over the past 18 years. Models predict that this trend is likely to change as atmospheric CO$_2$ concentrations continue to rise in the future [*Sarmiento et al.*, 1995]. As more CO$_2$ enters the ocean, the carbonate ion concentration will become depleted. This will decrease the buffering capacity of the ocean and its ability to continue carbon uptake at the current rate. Comparison of future survey cruises in the Indian Ocean with the anthropogenic and total carbon values from this study will allow us to document future changes in ocean chemistry and better understand the oceanic response to global change.

Finally, comparison of the spatial distribution of the anthropogenic carbon can be a powerful tool for understanding the carbon uptake of the models. The methods presented here provide a two-point calibration for examining the response of the models to
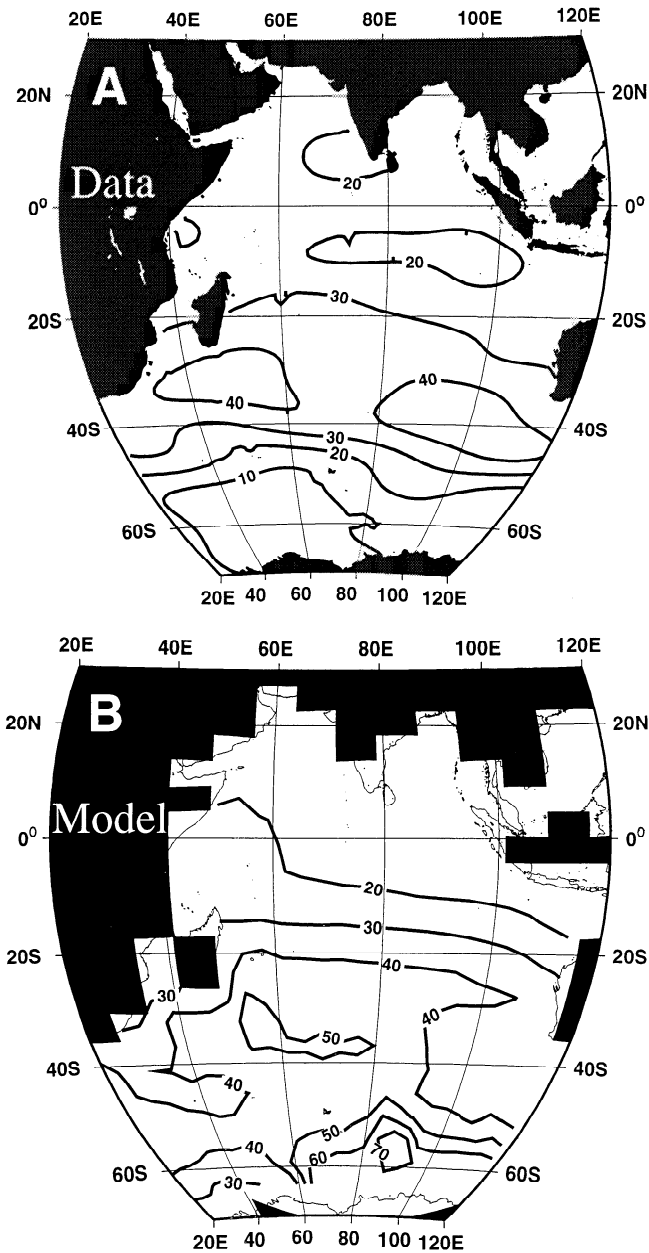
Figure 11. Maps of vertically integrated anthropogenic CO_2 based on (a) data and (b) model estimates. Contours are in mol m^{-2}. Solid regions indicate land mask used for inventory estimates. Thin lines in Figure 11b indicate land regions used in Figure 11a.

observed atmospheric CO_2 increases. The anthropogenic CO_2 data can also be subtracted from the TCO_2 measurements to provide an estimate of the preindustrial TCO_2 distribution. Comparing these estimates with the steady state model distributions can provide insight into whether differences in the model and data-based anthropogenic inventories result from problems with the uptake parameterization or the basic physics and initialization parameters of the model. This paper is just the first step in the interpretation of the WOCE/JGOFS data set. Subsequent papers will analyze additional cruise data as they become available. Together, these analyses will significantly improve our understanding of the global carbon cycle.

References

Anderson, L., and D. Dyrssen, Alkalinity and total carbonate in the Arabian Sea: Carbonate depletion in the Red Sea and Persian Gulf, *Mar. Chem.*, *47*, 195-202, 1994.

Anderson, L.A., and J.L. Sarmiento, Redfield ratios of remineralization determined by nutrient data analysis, *Global Biogeochem. Cycles*, *8*, 65-80, 1994.

Brewer, P.G., A.L. Bradshaw, and R.T. Williams, Measurement of total carbon dioxide and alkalinity in the North Atlantic Ocean in 1981, in *The Changing Carbon Cycle: A Global Analysis*, edited by J.R. Trabalka and D.E. Reichle, pp. 348-370, Springer-Verlag, New York, 1986.

Brewer, P.G., D.M. Glover, C. Goyet, and D.K. Shafer, The *pH* of the North Atlantic Ocean: Improvements to the global model for sound absorption in seawater, *J. Geophys. Res.*, *100*, 8761-8776, 1995.

Brewer, P.G., C. Goyet, and G. Freiderich, Direct observation of the oceanic CO_2 increase revisited, *Proc. Natl. Acad. Sci. U. S. A.*, *94*, 8308-8313, 1997.

Broecker, W.S., 'NO', a conservative water-mass tracer, *Earth Planet. Sci. Lett.*, *23*, 100-107, 1974.

Broecker, W.S., T. Takahashi, H.J. Simpson, and T.-H. Peng, Fate of fossil fuel carbon dioxide and the global carbon budget, *Science*, *206*, 409-418, 1979.

Bullister, J.L., and R.F. Weiss, Determination of CCl_3F and CCl_2F_2 in seawater and air, *Deep Sea Res., Part A*, *35*, 839-853, 1988.

Bullister, J.L., D.P. Wisegrave, W.M. Smethie, and M.J. Warner, The appearance of CFCs and carbon tetrachloride in the abyssal waters of the Samoa Passage, *Eos, Trans. AGU*, *79*, 1998.

Chen, C.-T., Rates of calcium carbonate dissolution and organic carbon decomposition in the North Pacific Ocean, *J. Oceanogr. Soc. Jpn.*, *46*, 201-210, 1990.

Chen, C.-T., and R.M. Pytkowicz, On the total CO_2-titration alkalinity-oxygen system in the Pacific Ocean, *Nature*, *281*, 362-365, 1979.

Chen, D.W., and C.-T. Chen, The anthropogenic CO_2 signals in the Indian Ocean, *J. Environ. Prot. Soc. Repub. China*, *12* (2), 46-65, 1989.

Cleveland, W.S., and S.J. Devlin, Locally-weighted regression: An approach to regression analysis by local fitting, *JASA J. Am. Stat. Assoc.*, *83*, 596-610, 1988.

Cleveland, W.S., E. Grosse, and W.M. Shyu, Local regression models, in *Statistical Models in S*, edited by J.M. Chambers and T.J. Hastie, pp. 309-376, Wadsworth and Brooks, Pacific Grove, California, 1992.

Culberson, C.H., et al., A comparison of methods for the determination of dissolved oxygen in seawater, *WHPO Rep. 91-2*, World Ocean Circ. Exp. Hydrogr. Programme Off., Woods Hole, Massachusetts, 1991.

Dickson, A.G., The ocean carbon dioxide system: Planning for quality data, *US JGOFS News*, 2(2), 2, 1990.

Doney, S.C., W.J. Jenkins, and J. Bullister, A comparison of ocean tracer dating techniques on a meridional section in the eastern North Atlantic, *Deep-Sea Res., Part I*, *44*, 603-626, 1997.

Dueser, W.G., E.H. Ross, and Z.J. Mlodzinska, Evidence for and rate of denitrification in the Arabian Sea, *Deep Sea Res.*, *25*, 431-445, 1978.

Edmond, J.M., High precision determination of titration alkalinity and total carbon dioxide content of seawater by potentiometric titration, *Deep Sea Res.*, *17*, 737-750, 1970.

England, M.H., Using chlorofluorocarbons to assess ocean climate models, *Geophys. Res. Lett.*, *22*, 3051-3054, 1995.

Gordon, L.I., J.C. Jennings Jr., A.A. Ross, and J.M. Krest, A suggested protocol for continuous flow automated analysis of seawater nutrients in the WOCE Hydrographic Programme and the Joint Global Ocean Fluxes Study, Grp. Tech. Rep. 92-1, Coll. of Oceanogr., Oregon State Univ., Corvallis, 1992.

Gruber, N., Anthropogenic CO$_2$ in the Atlantic Ocean, Global Biogeochem. Cycles, 12, 165-191, 1998.

Gruber, N., and J.L. Sarmiento, Global patterns of marine nitrogen fixation and denitrification, Global Biogeochem. Cycles, 11, 235-266, 1997.

Gruber, N., J.L. Sarmiento, and T.F. Stocker, An improved method for detecting anthropogenic CO$_2$ in the oceans, Global Biogeochem. Cycles, 10, 809-837, 1996.

Johnson, K.M., A.E. King, and J.M. Sieburth, Coulometric TCO$_2$ analyses for marine studies: An introduction, Mar. Chem., 16, 61-82, 1985.

Johnson, K.M., et al., Coulometric total carbon dioxide analysis for marine studies: Assessment of the quality of total inorganic carbon measurements made during the US Indian Ocean CO$_2$ Survey 1994-1996, Mar. Chem., 63, 21-37, 1998.

Keeling, C.D., and T.P. Whorf, Atmospheric CO$_2$ records from sites in the SIO air sampling network, in Trends: A Compendium of Data on Global Change, Carbon Dioxide Inf. Anal. Cent., Oak Ridge Nat. Lab., Oak Ridge, Tenn., 1996.

Keeling, C.D., S.C. Piper, and M. Heimann, A three-dimensional model of atmospheric CO$_2$ transport based on observed winds, 4, Mean annual gradients and interannual variations, in Aspects of Climate Variability in the Pacific and the Western Americas, Geophys. Monogr. Ser., Vol. 55, edited by D.H. Peterson, pp. 305-363, AGU, Washington D.C., 1989.

Keeling, R.F., and S.R. Shertz, Seasonal and interannual variations in atmospheric oxygen and implications for the global carbon cycle, Nature, 358, 723-727, 1992.

Leboucher, V., J. Orr, P. Jean-Baptiste, M. Arnold, P. Monfray, N. Tisnerat-Laborde, A. Poisson, and J. Duplessy, Oceanic radiocarbon between Antarctica and South Africa along WOCE section I6 at 30°E, Radiocarbon, in press, 1998.

Levitus, S., and T.P. Boyer, Temperature, in NOAA Atlas NESDIS 3: World Ocean Atlas 1994, NOAA Tech. Rep. 4, Natl. Environ. Satell. Data and Inf. Serv., Silver Spring, MD, 1994.

Levitus, S., R. Burgett, and T.P. Boyer, Salinity, in NOAA Atlas NESDIS 3: World Ocean Atlas 1994, NOAA Tech. Rep. 3, Natl. Environ. Satell. Data and Inf. Serv., Silver Spring, MD, 1994.

Merbach, C., C.H. Culberson, J.E. Hawley, and R.M. Pytkowicz, Measurements of the apparent dissociation constants of carbonic acid in seawater at atmospheric pressure, Limnol. Oceanogr., 18, 897-907, 1973.

Millard, R.C., Jr., CTD calibration and data processing techniques at WHOI using the practical salinity scale, paper presented at International STD Conference and Workshop, Mar. Tech. Soc., La Jolla, Calif., 1982.

Millero, F.J., et al., Total alkalinity measurements in the Indian Ocean during the WOCE Hydrographic Program CO$_2$ survey cruises 1994-1996, Mar. Chem., 63, 9-20, 1998a.

Millero, F.J., K. Lee, and M. Roche, Alkalinity as a major variable in the marine carbonate system, Mar. Chem., 60, 111-130, 1998b.

Murnane, R., J.L. Sarmiento, and C. LeQuere, The spatial distribution of air-sea CO$_2$ fluxes and the interhemispheric transport of carbon by the oceans, Global Biogeochem. Cycles, in press, 1999.

Murphy, P.P., R.A. Feely, R.H. Gammon, K.C. Kelly, and L.S. Waterman, Autumn air-sea disequilibrium of CO$_2$ in the South Pacific Ocean, Mar. Chem., 35, 77-84, 1991.

Naqvi, S.W.A., and R. Sen Gupta, "NO" a useful tool for the estimation of nitrate deficits in the Arabian Sea, Deep Sea Res., Part A, 32, 665-674, 1985.

Neftel, A., H. Friedli, E. Moor, H. Lotscher, H. Oeschger, U. Siegenthaler, and B. Stauffer, Historical CO$_2$ record from the Siple station ice core, in Trends '93: A Compendium of Data on Global Change, edited by T. Boden et al., Rep. ORNL/CDIAC-65, pp. 11-14, Carbon Dioxide Inf. Anal. Cent., Oak Ridge Nat. Lab., Oak Ridge, Tenn., 1994.

Papaud, A., and A. Poisson, Distribution of dissolved CO$_2$ in the Red Sea and correlation with other geochemical tracers, J. Mar. Res., 44, 385-402, 1986.

Poisson, A., and C.-T.A. Chen, Why is there little anthropogenic CO$_2$ in the Antarctic Bottom Water?, Deep Sea Res., Part A, 34, 1255-1275, 1987.

Poisson, A., B. Schauer, and C. Brunet, Les Rapports des campagnes a la

mer, MD43/INDIGO 1, in Les publications de la mission de recherche des Terres Australes et Antarctiques Fancaises, Rep. 85-06, 267 pp., Univ. Pierre et Marie Curie, Paris, France, 1988.

Poisson, A., B. Schauer and C. Brunet, Les Rapports des campagnes a la mer, MD49/INDIGO 2, in Les publications de la mission de recherche des Terres Australes et Antarctiques Fancaises, Rep. 86-02, 234 pp., Univ. Pierre et Marie Curie, Paris, France, 1989.

Poisson, A., B. Schauer and C. Brunet, Les Rapports des campagnes a la mer. MD53/INDIGO 3, in Les publications de la mission de recherche des Terres Australes et Antarctiques Fancaises, Rep. 87-02, 269 pp., Univ. Pierre et Marie Curie, Paris, France, 1990.

Quay, P.D., B. Tilbrook, and C.S. Wong, Oceanic uptake of fossil fuel CO$_2$: Carbon-13 evidence, Science, 256, 74-79, 1992.

Sarmiento, J.L., and E.T. Sundquist, Revised budget for the oceanic uptake of anthropogenic carbon dioxide, Nature, 356, 589-593, 1992.

Sarmiento, J.L., J. Willebrand, and S. Hellerman, Objective analysis of Tritium observations in the Atlantic Ocean during 1971-74, OTL Tech Rep. 1, 19 pp., Ocean Tracers Lab., Princeton Univ., Princeton, N. J., 1982.

Sarmiento, J.L., J.C. Orr, and U. Siegenthaler, A perturbation simulation of CO$_2$ uptake in an ocean general circulation model, J. Geophys. Res., 97, 3621-3645, 1992.

Sarmiento, J.L., R. Murnane, and C. LeQuere, Air-sea CO$_2$ transfer and the carbon budget of the North Atlantic, Philos. Trans. R. Soc. London, Ser. B, 348, 211-219, 1995.

Sen Gupta, R., M.D. Rajagopal, and S.Z. Qasim, Relationship between dissolved oxygen and nutrients in the northwestern Indian Ocean, Indian J. Mar. Sci., 5, 201-211, 1976.

Siegenthaler, U., and F. Joos, Use of a simple model for studying oceanic tracer distributions and the global carbon cycle, Tellus, Ser. B, 44, 186-207, 1992.

Siegenthaler, U., and J.L. Sarmiento, Atmospheric carbon dioxide and the ocean, Nature, 365, 119-125, 1993.

Stocker, T.F., W.S. Broecker, and D.G. Wright, Carbon uptake experiments with a zonally-averaged global circulation model, Tellus, Ser. B, 46, 103-122, 1994.

Takahashi, T.T., R.A. Feely, R.F. Weiss, R.H. Wanninkhof, D.W. Chipman, S.C. Sutherland, and T.T. Takahashi, Global air-sea flux of CO$_2$: An estimate based on measurements of sea-air pCO$_2$ difference, Proc. Natl. Acad. Sci. U. S. A., 94, 8292-8299, 1997.

Tans, P.P., I.Y. Fung, and T. Takahashi, Observational constraints on the global atmospheric CO$_2$ budget, Science, 247, 1431-1438, 1990.

Toggweiler, J.R., K. Dickson, and K. Bryan, Simulations of radiocarbon in a coarse-resolution world ocean model, 1. Steady state pre-bomb distributions, J. Geophys. Res., 94, 8217-8242, 1989.

UNESCO, Background papers and supporting data on the Practical Salinity Scale, 1978 UNESCO Tech. Pap. in Mar. Sci., 37, 1981.

Wallace, D.W.R., Monitoring global ocean inventories, OOSDP Background Rep. 5, 54 pp., Ocean Observ. Syst. Dev. Panel, Texas A&M Univ., College Station, Tex., 1995.

Warner, M.J. and R.F. Weiss, Solubilities of chlorofluorocarbons 11 and 12 in water and seawater, Deep-Sea Res., 32, 1485-1497, 1985.

Warner, M.J., J.L. Bullister, D.P. Wisegarver, R.H. Gammon, and R.F. Weiss, Basin-wide distributions of chlorofluorocarbons CFC-11 and CFC-12 in the North Pacific: 1985-1989, J. Geophys. Res., 101, 20525-20542, 1996.

Weiss, R.F., W.S. Broecker, H. Craig, and D. Spencer, GEOSECS Indian Ocean Expedition Vol. 5, Hydrographic Data 1977-1978, 48 pp., Natl. Sci. Found., U.S. Gov. Print. Off., Washington D. C., 1983.

Wessel, P., and W.H.F. Smith, New version of generic mapping tools released, Eos Trans. AGU, 76, 329, 1995.

Wyrtki, K., Physical oceanography of the Indian Ocean, in Ecological Studies: Analysis and Synthesis, vol. 3, pp. 18-36, edited by B. Zeitzschel, Springer-Verlag, New York, 1973.

K.M. Johnson, Oceanographic and Atmospheric Sciences Division, Brookhaven National Laboratory, Upton, NY 11973.

R.M. Key, C.L. Sabine, and J.L. Sarmiento, Department of Geosciences, Princeton University, Princeton, NJ 08544. (key@geo.princeton.edu, sabine@geo.princeton.edu, and jls@splash.princeton.edu)

F.J. Millero, Rosensticl School of Marine and Atmospheric Sciences, University of Miami, 4600 Rickenbacker Cswy., Miami, FL 33149. (fmillero@rsmas.miami.edu)

A. Poisson, Laboratoire de Physique et Chimie Marines, Université Pierre et Marie Curie, 4 Place Jussieu, Tour 24-25, 75720 Paris Cedex 05 France. (apoisson@ccr.jussieu.fr)

D.W.R. Wallace, Abteilung Meereschemie, Institut für Meereskunde an der Universität Kiel, Duesternbrooker Weg 20, D-24105 Kiel, Germany. (dwallace@ifm.uni-kiel.de)

C.D. Winn, Marine Science Program, Hawaii Pacific University, 45-045 Kamehameha Highway, Kaneohe, HI 96744-5297. (cwinn@soest.hawaii.edu)